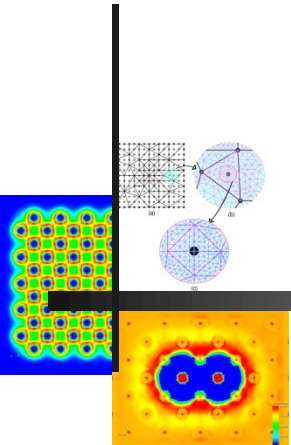


Fast, Accurate and Large-scale Ab-initio Calculations for Materials Simulations



Vikram Gavini

Department of Mechanical Engineering

Department of Materials Science & Engineering

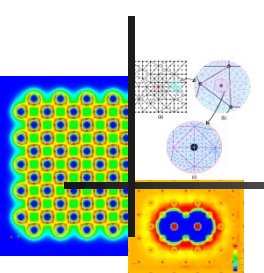
Program in Applied Physics

University of Michigan, Ann Arbor

*Collaborators: Sambit Das (U. Mich.), Bikash Kanungo (U. Mich.),
Phani Motamarri (IISc)*

Funding: DoE-BES, TRI, NERSC, OLCF





Quantum Mechanics

- Schrödinger equation - $H\psi = E\psi$

$$H = -\frac{1}{2} \sum_{i=1}^N \nabla_i^2 - \frac{1}{2} \sum_{A=1}^M \frac{1}{M_A} \nabla_A^2 - \sum_{i=1}^N \sum_{A=1}^M \frac{Z_A}{|\mathbf{r}_i - \mathbf{R}_A|} \\ + \sum_{i=1}^N \sum_{j>i}^N \frac{1}{|\mathbf{r}_i - \mathbf{r}_j|} + \sum_{A=1}^M \sum_{B=1, B>A}^M \frac{Z_A Z_B}{|\mathbf{R}_A - \mathbf{R}_B|}$$

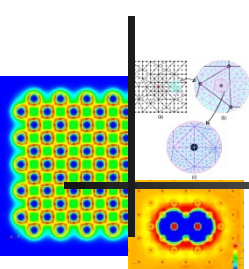
$$\psi = \psi(\mathbf{x}_1, \mathbf{x}_2, \dots, \mathbf{x}_N, \mathbf{R}_1, \mathbf{R}_2, \dots, \mathbf{R}_M)$$

- Born-Oppenheimer approximation - Classical treatment of atomic nuclei

$$\psi = \psi(\mathbf{x}_1, \mathbf{x}_2, \dots, \mathbf{x}_N)$$

- Computational complexity - $\psi \in \mathbf{R}^{3N}$!!





Density-functional theory – Kohn-Sham approach

- Ground-state energy is a functional of electron-density !! (Kohn & Sham, 1964-65)

$$\langle \psi | H | \psi \rangle \geq E_0 \quad (\text{Variational statement})$$

$$\begin{aligned}
 E_0 &= \min_{\psi} \langle \psi | T + \frac{1}{2} \sum_i \sum_j' \frac{1}{|\mathbf{r}_i - \mathbf{r}_j|} + \sum_i V_{ext}(\mathbf{r}_i) | \psi \rangle + E_{zz} \\
 &= \min_{\psi} \langle \psi | T + \frac{1}{2} \sum_i \sum_j' \frac{1}{|\mathbf{r}_i - \mathbf{r}_j|} | \psi \rangle + \int \rho(\mathbf{r}) V_{ext}(\mathbf{r}) d\mathbf{r} + E_{zz} \\
 &= \min_{\rho} \left\{ \underbrace{\left(\min_{\psi \rightarrow \rho} \langle \psi | T + \frac{1}{2} \sum_i \sum_j' \frac{1}{|\mathbf{r}_i - \mathbf{r}_j|} | \psi \rangle \right)}_{F(\rho)} + \int \rho(\mathbf{r}) V_{ext}(\mathbf{r}) d\mathbf{r} \right\} + E_{zz}
 \end{aligned}$$

$$F(\rho) = T_s(\rho) + E_H(\rho) + E_{xc}(\rho) \longrightarrow$$

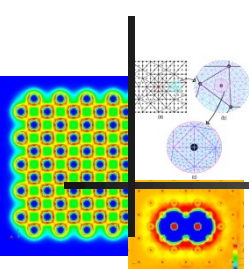
↓

Exchange-correlation
functional: Model using
LDA, GGA

Kinetic energy of non-interacting electrons:
Computed from wave-functions of the
resulting E-L eqn.



Density Functional Theory



Kohn-Sham eigenvalue problem:

$$\left(-\frac{1}{2}\nabla^2 + V_{\text{eff}}[\rho; \mathbf{R}] \right) \psi_i = \epsilon_i \psi_i \quad \Downarrow \quad \boxed{\begin{array}{l} \text{Self Consistent Field (SCF) iteration} \\ (\text{Kohn-Sham map}) \end{array}}$$

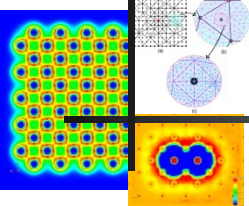
$$V_{\text{eff}}[\rho; \mathbf{R}] = V_{\text{ext}}(\mathbf{R}) + V_H(\rho) + V_{xc}(\rho) \quad \rho(\mathbf{r}) = 2 \sum_i f_i |\psi_i(\mathbf{r})|^2$$

$$T_s(\Psi) = \frac{1}{2} \sum_i f_i \int |\nabla \psi_i(\mathbf{r})|^2 d\mathbf{r} \quad E_0(\Psi) = T_s(\Psi) + E_{xc}(\rho) + E_H(\rho) + E_{ext}(\rho) + E_{zz}$$

Remarks:

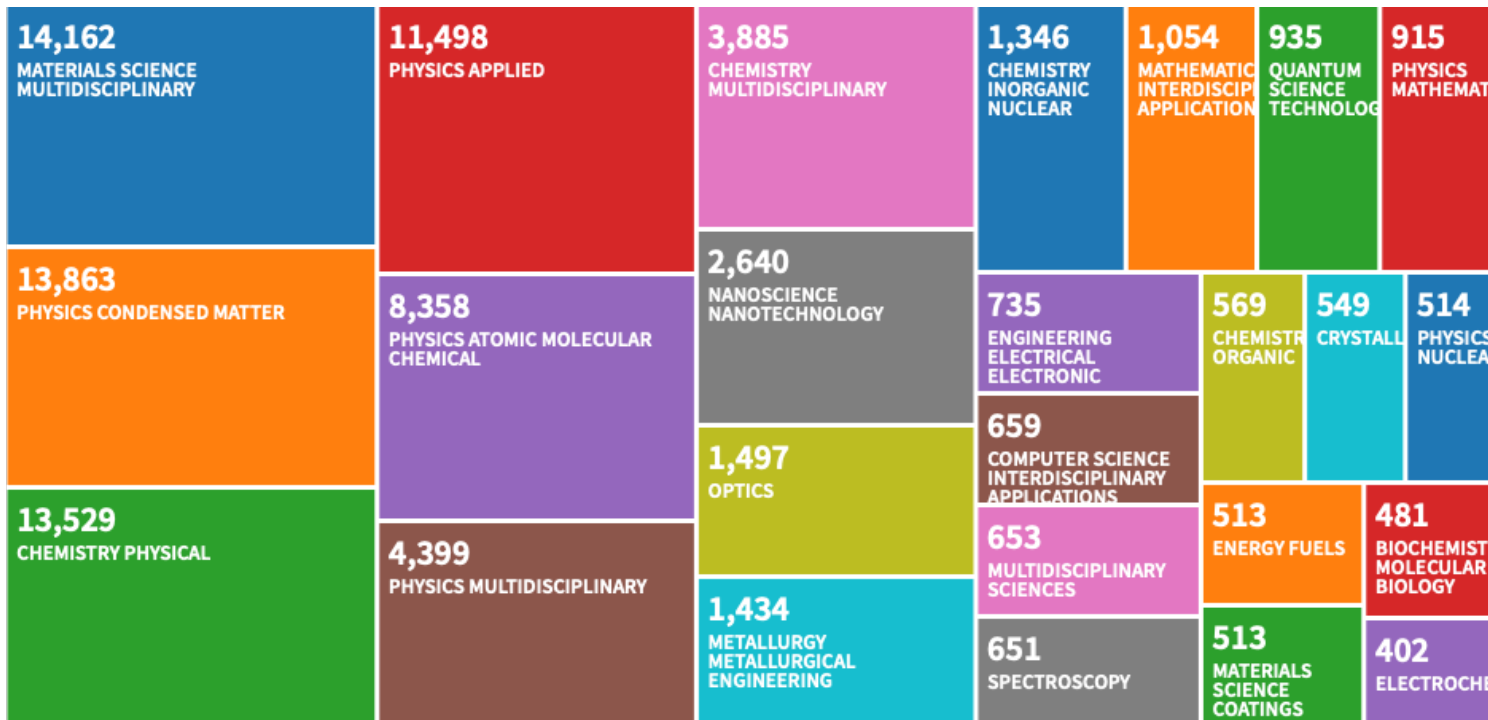
- Ground-state energy; structure -> Range of Material Properties
- The most computational intensive step in each SCF iteration is the solution of the eigenvalue problem
 - ❖ Computational complexity scales as $O(N^3)$





Impact of Density Functional Theory

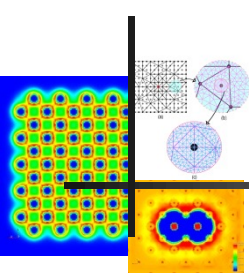
Citations to seminal work of Walter Kohn (1964,1965)



Data compiled from Web of Science

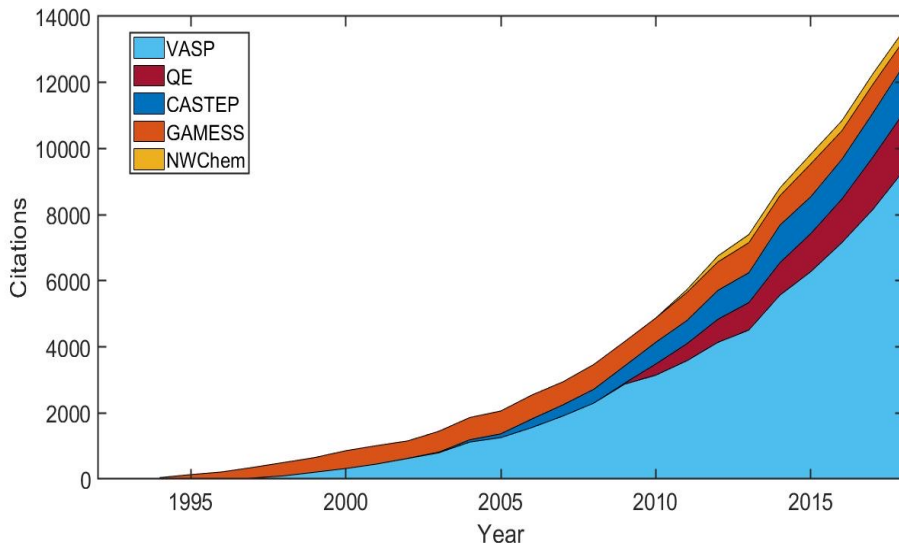
12 of the 100 most-cited papers in scientific literature pertain to DFT!
(Nature 514, 550 (2014))





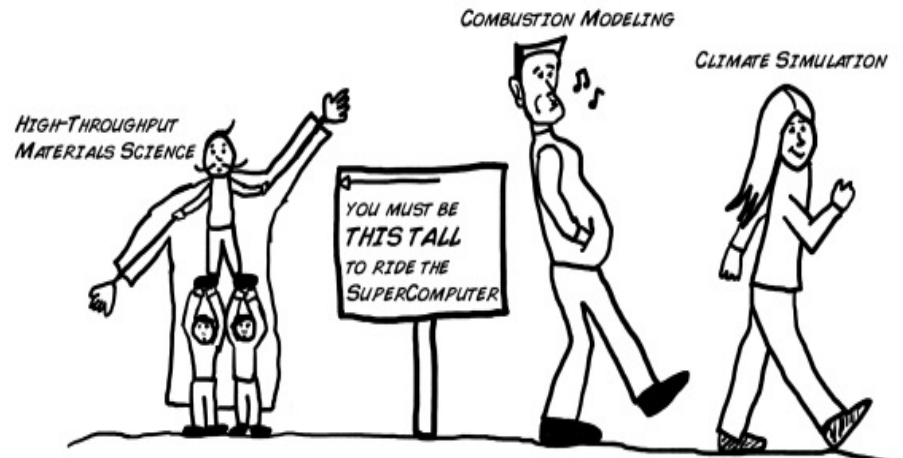
DFT codes

~100 available DFT codes developed since 1980



Data compiled from Web of Science

Relationship to HPC

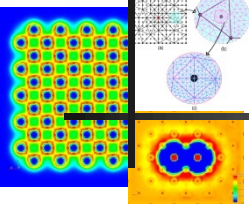


Courtesy: Anubhav Jain

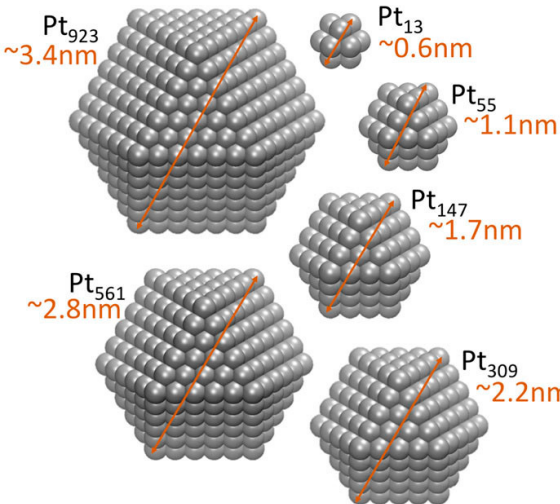
Key Issues

- ❖ Lack of good parallel scalability of existing DFT codes
- ❖ Computational complexity of DFT calculations ($O(N^3)$)

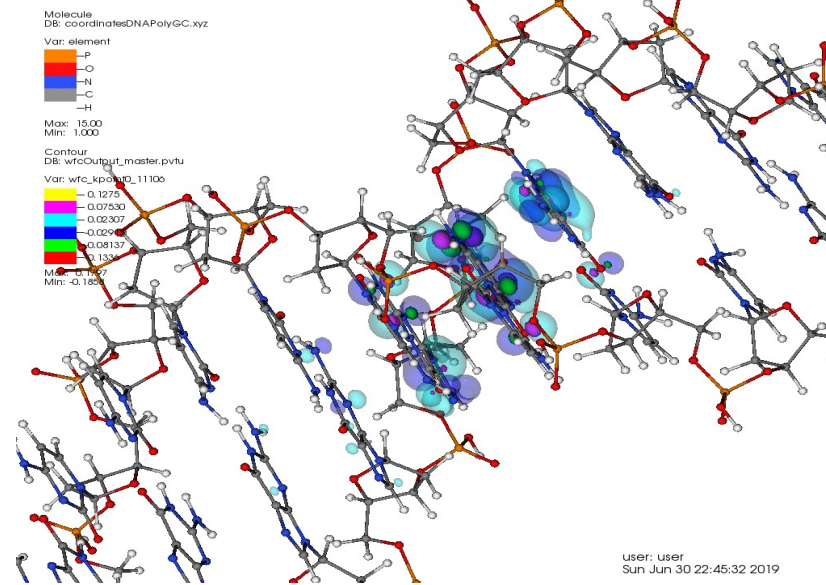




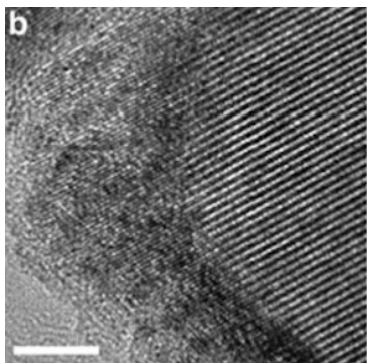
Need for large scale DFT calculations



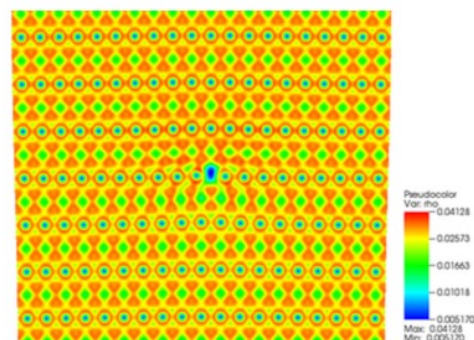
Chemical properties of nanoparticles



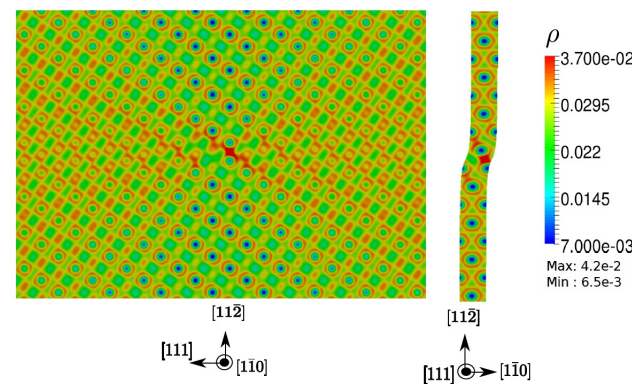
Biological systems



Rocksalt phase formation during Litihiation of Magnetite
He et. al, Nature Comm, 2016

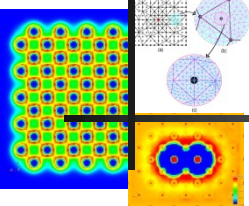


Edge dislocation:
Iyer et al. J. Mech, Phys. Solids (2015)



Screw dislocation:
Das & Gavini J. Mech, Phys. Solids (2017)





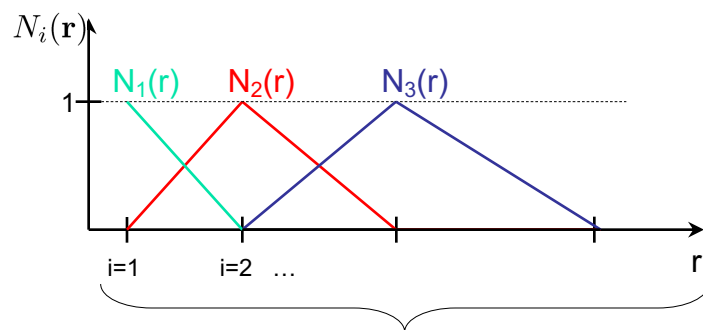
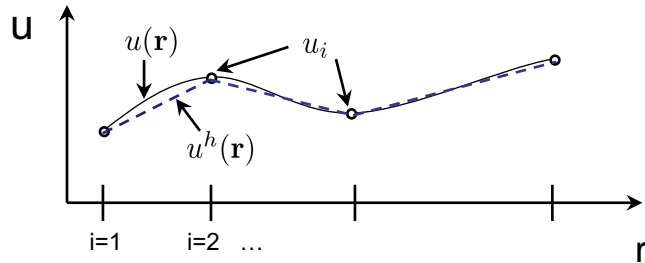
DFT – Finite Element discretization

- Use finite-element basis for computing –

$$\psi_i^h(\mathbf{r}) = \sum_k \psi_{ik} N_k(\mathbf{r}) \quad i = 1, 2, \dots, N$$

ψ_{ik} – Nodal values

$N_k(\mathbf{r})$ – Shape functions



By changing the positioning of the nodes the spatial resolution of basis can be changed/adapted

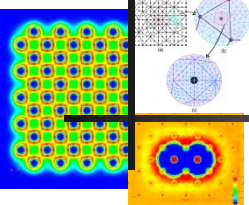
Features of FE basis

- Systematic convergence
 - ❖ Element size
 - ❖ Polynomial order
- Adaptive refinement
- Complex geometries and boundary conditions
- Potential for excellent parallel scalability

White et al. (1989); Tuschida & Tsukada (1995); Pask et al. (1999); Pask et al. (2001) [and many others]

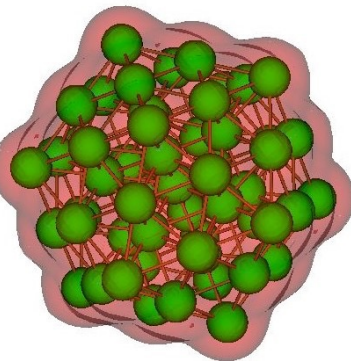
But ... **huge degree of freedom disadvantage!**



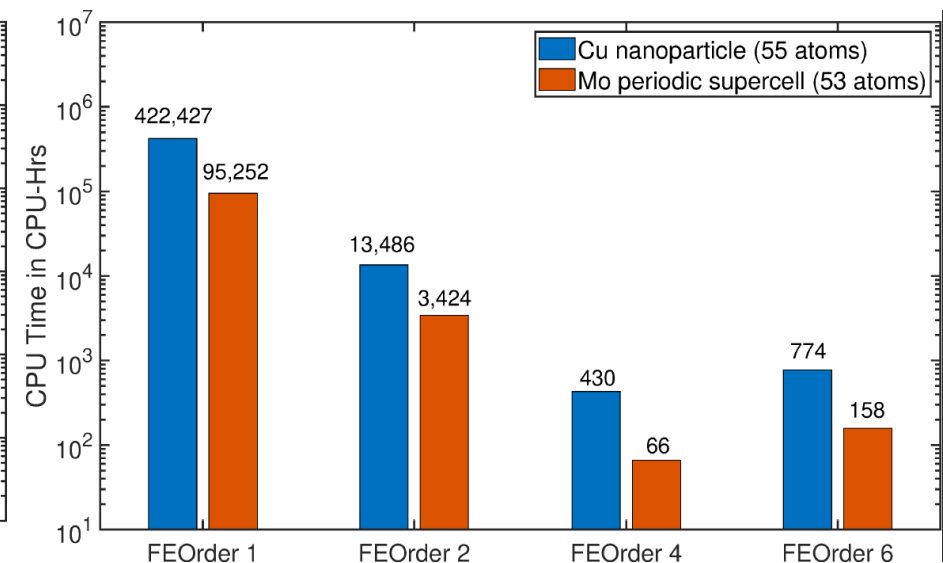
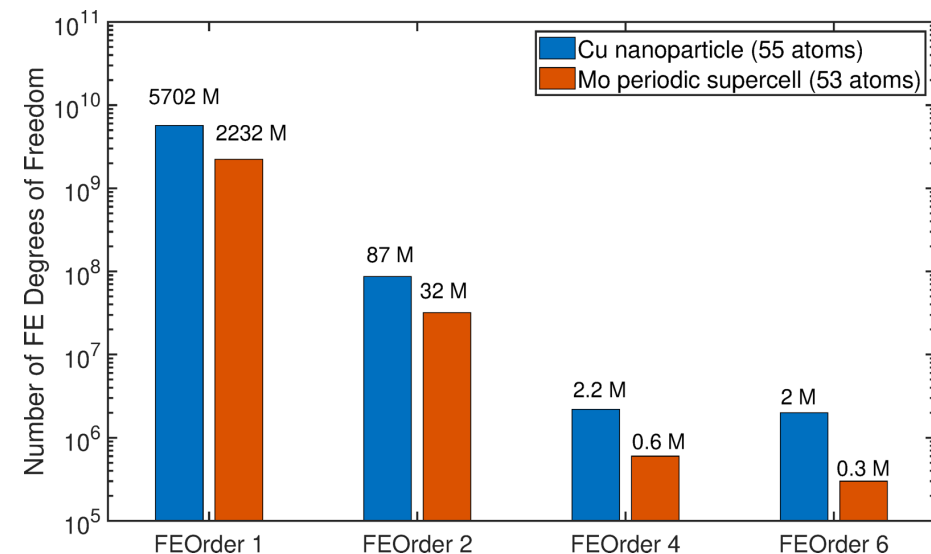
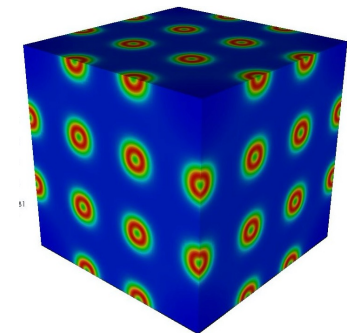


Higher (polynomial) order FE basis

I. Cu nanoparticle
55 atoms

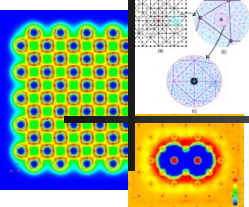


II. Mo periodic
supercell w/ vacancy
53 atoms



~1000x advantage by using higher-order FE basis !

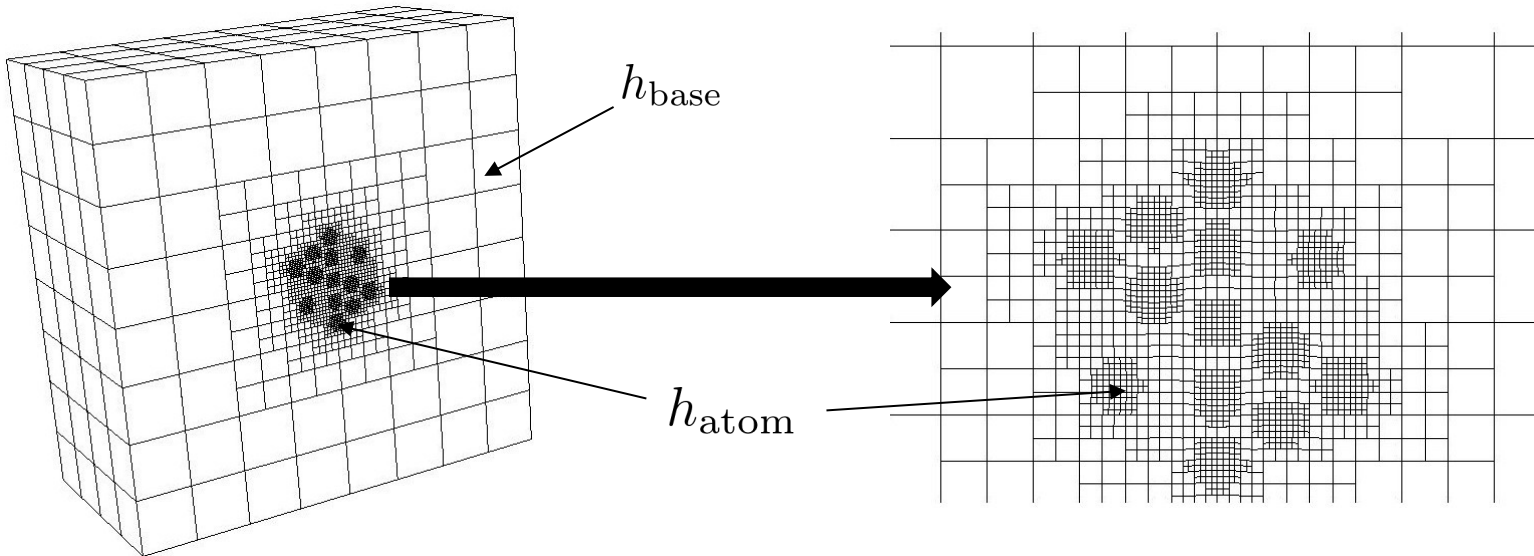




Spatial adaptivity of the FE basis

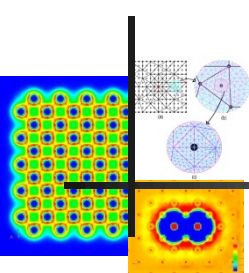
(Motamarri et al. J Comput Phys. (2013); Motamarri et al. Comput. Phys. Commun. (2020))

- Error Analysis: $|E - E^h| \leq C \left(\sum_i |\bar{\psi}_i - \bar{\psi}_i^h|_{1,\Omega}^2 \right) \leq \mathcal{C} \sum_e h_e^{2k} \left[\sum_i |\bar{\psi}_i|_{k+1,\Omega_e}^2 \right]$
- Optimal FE mesh: $\min_h \int_{\Omega} \left\{ h^{2k}(\mathbf{r}) \left[\sum_i |D^{k+1} \bar{\psi}_i(\mathbf{r})|^2 \right] \right\} d\mathbf{r}$ subject to $\int_{\Omega} \frac{d\mathbf{r}}{h^3(\mathbf{r})} = N_E$



System Type pyr II dislocation	DoFs Uniform Mesh	DoFs for Adaptive Mesh
1848 atom Mg	347,206,614	55,112,161
6164 atom Mg	892,047,315	179,034,231





DFT – FE discretization

- Discrete eigenvalue problem:

$$\mathbf{H}\hat{\psi}_k = \varepsilon_k^h \mathbf{M}\hat{\psi}_k$$

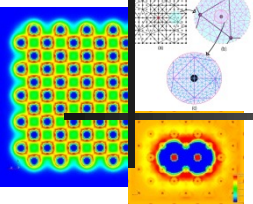
$$\begin{aligned}\mathbf{H}_{ij} &= \frac{1}{2} \int_{\Omega} \nabla N_i(\mathbf{r}) \cdot \nabla N_j(\mathbf{r}) d\mathbf{r} + \int_{\Omega} V_{eff}(\mathbf{r}, \mathbf{R}) N_i(\mathbf{r}) N_j(\mathbf{r}) d\mathbf{r} \\ \mathbf{M}_{ij} &= \int_{\Omega} N_i(\mathbf{r}) N_j(\mathbf{r}) d\mathbf{r}\end{aligned}$$

- Transformation to a standard eigenvalue problem:

$$\tilde{\mathbf{H}}\tilde{\psi}_k = \varepsilon_k^h \tilde{\psi}_k \quad \text{where} \quad \tilde{\mathbf{H}} = \mathbf{M}^{-1/2} \mathbf{H} \mathbf{M}^{-1/2} \quad \text{and} \quad \tilde{\psi}_k = \mathbf{M}^{1/2} \hat{\psi}_k$$

- Remark: $\tilde{\mathbf{H}}$ denotes the projection of the Hamiltonian operator into a space spanned by Löwden orthonormalized finite-element basis

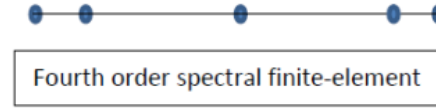




Spectral FE basis and Gauss-Lobatto-Legendre quadrature

➤ *Spectral FE basis functions:*

- ❖ Constructed from Lagrange polynomials through nodes corresponding to the roots of the derivatives of the Legendre polynomials and boundary nodes (GLL points)



- ❖ Upon using a Gauss-Lobatto-Legendre quadrature rule, the quadrature points coincide with the FE nodes

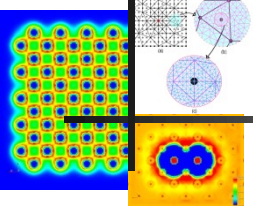


$$\mathbf{M}_{ij} = \int_{\Omega_e} N_i(\mathbf{r}) N_j(\mathbf{r}) d\mathbf{r} = C_i \delta_{ij}$$

➤ *Remarks:*

- ❖ Transformation to standard eigenvalue problem is trivial
- ❖ The reduced order quadrature rule is only employed for the computation of the overlap matrix, and the full Gauss quadrature is employed to compute the Hamiltonian matrix.

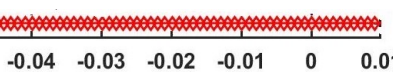
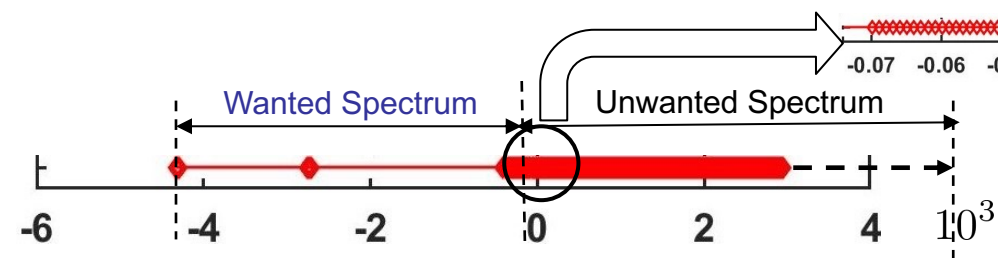




Eigen-space computation: Chebyshev acceleration

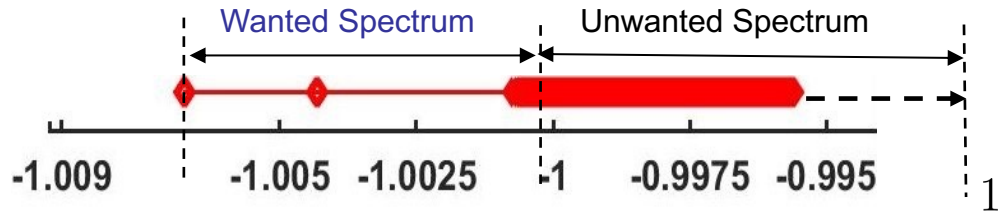
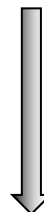
(Zhou et al. J. Comput. Phys. 219 (2006); Motamarri et al. J. Comp. Phys. 253, 308-343 (2013))

Kohn-Sham eigenvalue problem: $\tilde{\mathbf{H}}\tilde{\psi}_k = \epsilon_k \tilde{\psi}_k$ for $k = 1, 2, \dots, N$ ($N \sim 1.2N_e/2$)

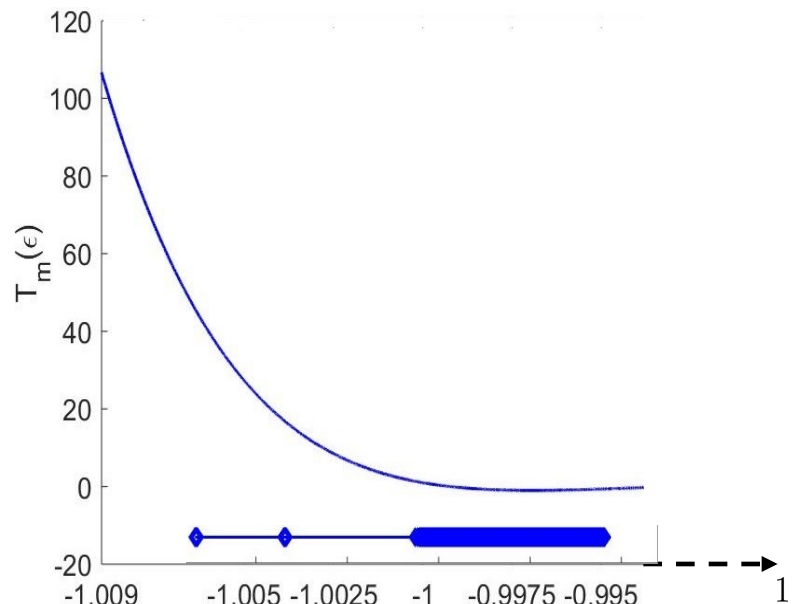


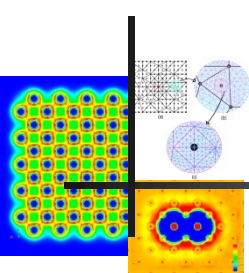
Chebyshev Filtering: $T_m(\bar{\mathbf{H}})\tilde{\Psi} = \tilde{\Psi}_F$

$$\bar{\mathbf{H}} = c_1 \tilde{\mathbf{H}} + c_2$$



$$T_m(\bar{\mathbf{H}})\mathbf{X} = [2\bar{\mathbf{H}}T_{m-1}(\bar{\mathbf{H}}) - T_{m-2}(\bar{\mathbf{H}})]\mathbf{X}$$

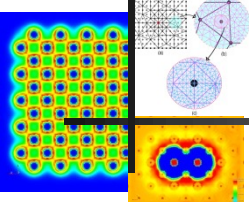




Numerical algorithm

1. Start with initial guess for electron density $\rho_{in}^h(\mathbf{r}) = \rho_0(\mathbf{r})$ and the initial wavefunctions
2. Compute the discrete Hamiltonian $\tilde{\mathbf{H}}$ using the input electron density ρ_{in}^h
3. **CF:** Chebyshev filtering: $\tilde{\Psi}_F = T_m(\bar{\mathbf{H}})\tilde{\Psi}$
4. **Orthonormalize** CF basis: $\tilde{\Psi}_F \rightarrow \tilde{\Psi}_F^o$
5. **Rayleigh-Ritz procedure:**
 - ❖ Compute projected Hamiltonian: $\hat{\mathbf{H}} = \tilde{\Psi}_F^{o\dagger} \tilde{\mathbf{H}} \tilde{\Psi}_F^o$
 - ❖ Diagonalize $\hat{\mathbf{H}}$: $\hat{\mathbf{H}}\mathbf{Q} = \mathbf{Q}\mathbf{D}$
 - ❖ Subspace rotation: $\tilde{\Psi}^R = \tilde{\Psi}_F^o \mathbf{Q}$
6. Compute electron density $\rho_{out}^h(\mathbf{r}) = 2 \sum_{i=1}^N f(\epsilon_i^h, \mu) |\psi_i^h(\mathbf{r})|^2$
7. If $||\rho_{out}^h(\mathbf{r}) - \rho_{in}^h(\mathbf{r})|| < tol$, EXIT; else, compute new ρ_{in}^h using a mixing scheme and go to (2).

Chebyshev Filtering

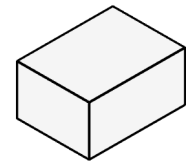
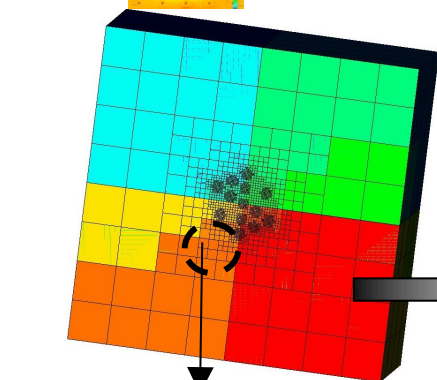


$$\mathbf{Y} = \mathbf{H} \mathbf{X}$$

$\mathbf{H} \rightarrow$ Sparse Matrix ($M \times M$)

$\mathbf{X} \rightarrow$ Dense Matrix ($M \times N$)

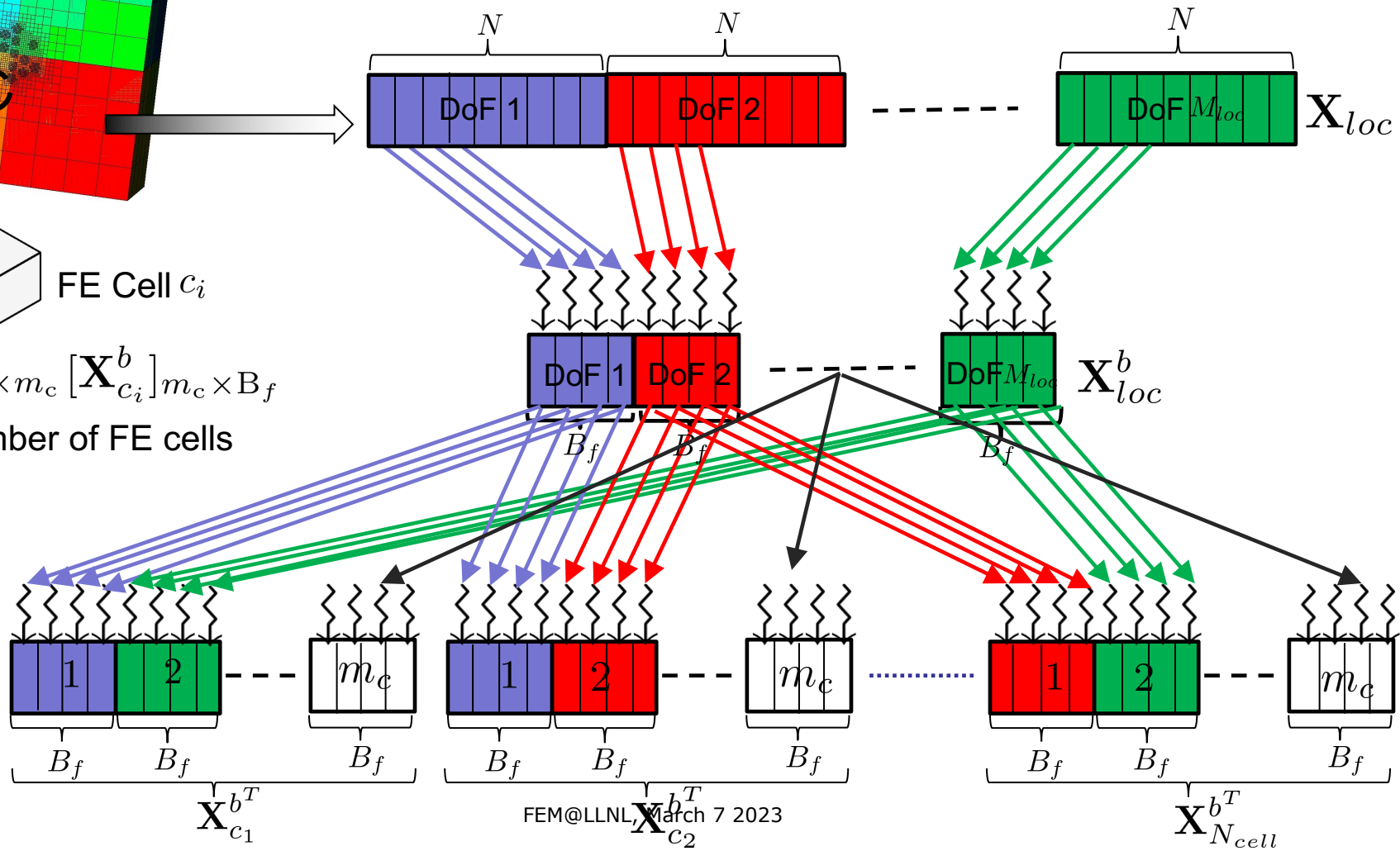
$\mathbf{Y} \rightarrow$ Dense Matrix ($M \times N$)



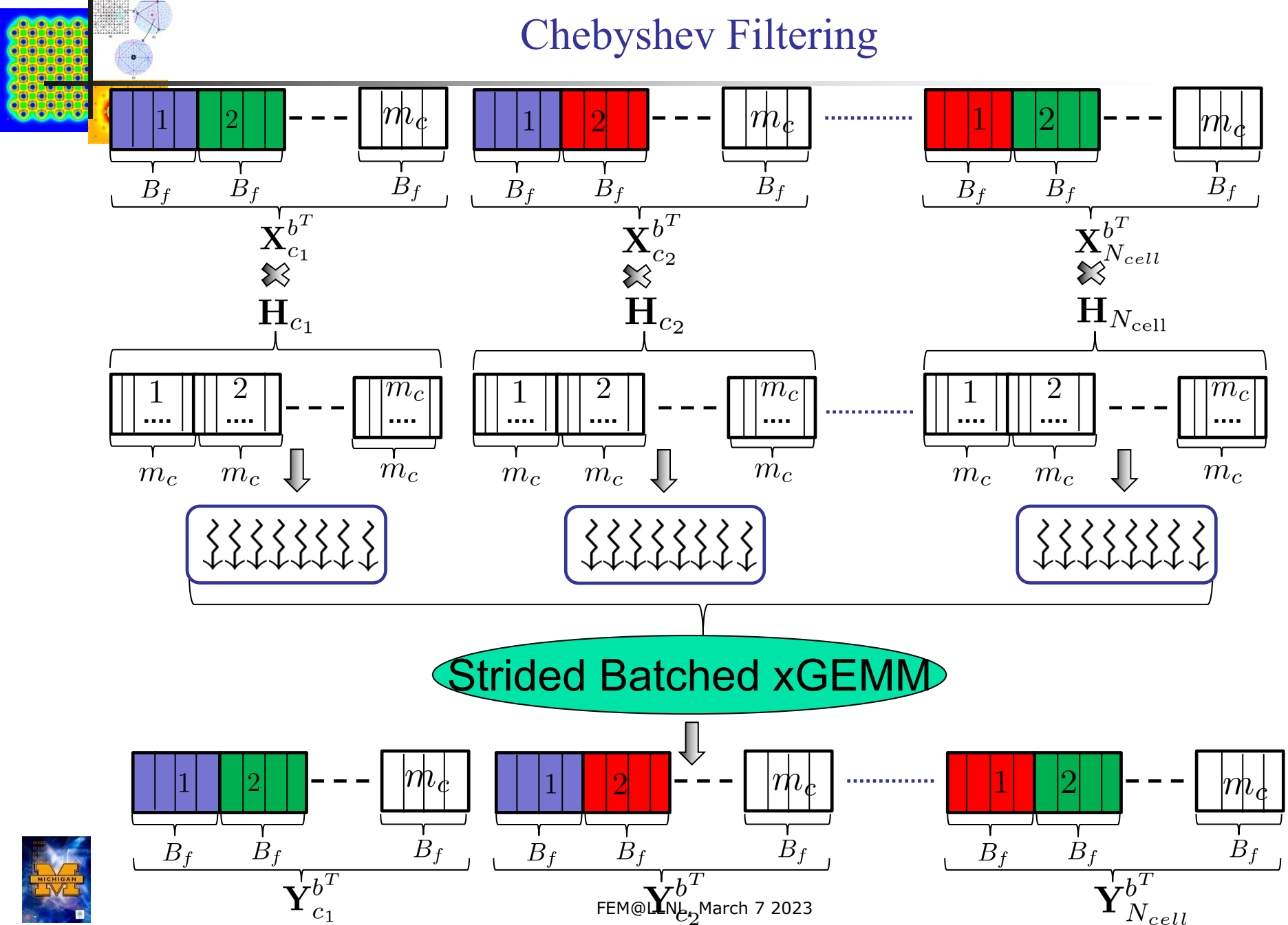
FE Cell c_i

$[\mathbf{H}_{c_i}]_{m_c \times m_c}$ $[\mathbf{X}_{c_i}^b]_{m_c \times B_f}$

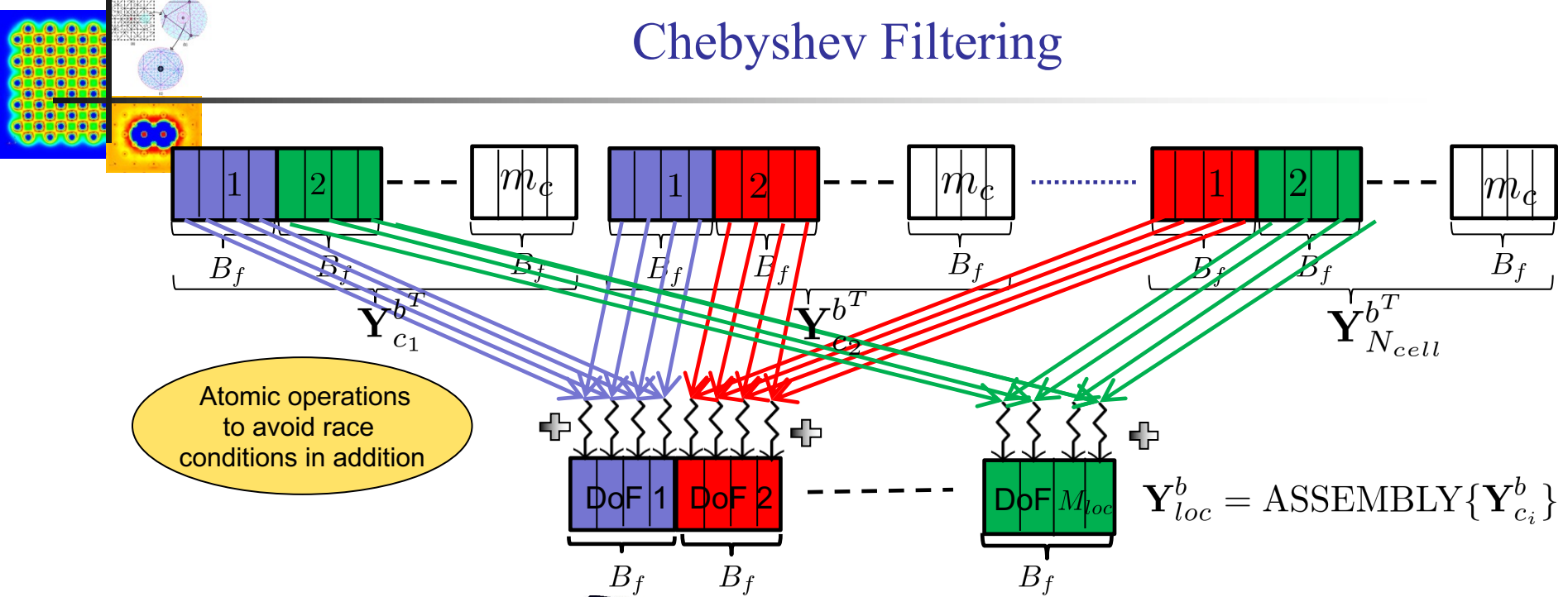
N_{cell} : Number of FE cells



Chebyshev Filtering

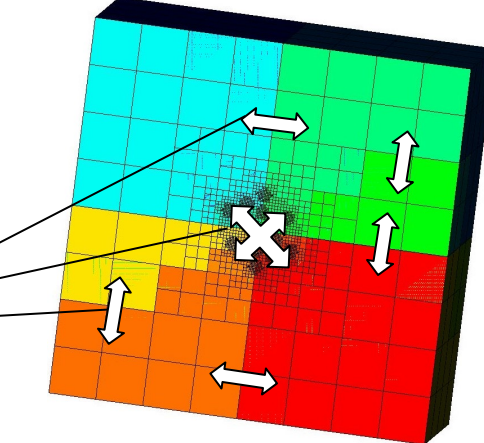


Chebyshev Filtering



$$\mathbf{Y}^b = \text{ASSEMBLY}\{\mathbf{Y}_{loc}^b\}$$

Assembly across processor boundaries: Communication in FP32

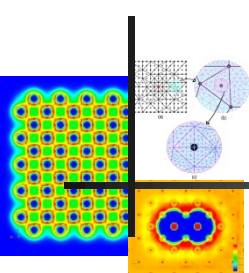


Blocked approach allows overlapping compute of one block with communication of another block

$$\mathbf{Y}^b = T_m(\mathbf{H})\mathbf{X}^b = [2\mathbf{H}T_{m-1}(\mathbf{H}) - T_{m-2}(\mathbf{H})]\mathbf{X}^b$$

Repeat for $b = 1 \dots \frac{N}{B_f}$





Performance of Chebyshev filtering (Summit)

Case study: Mg 3x3x3 supercell with a vacancy. (1070 electrons)

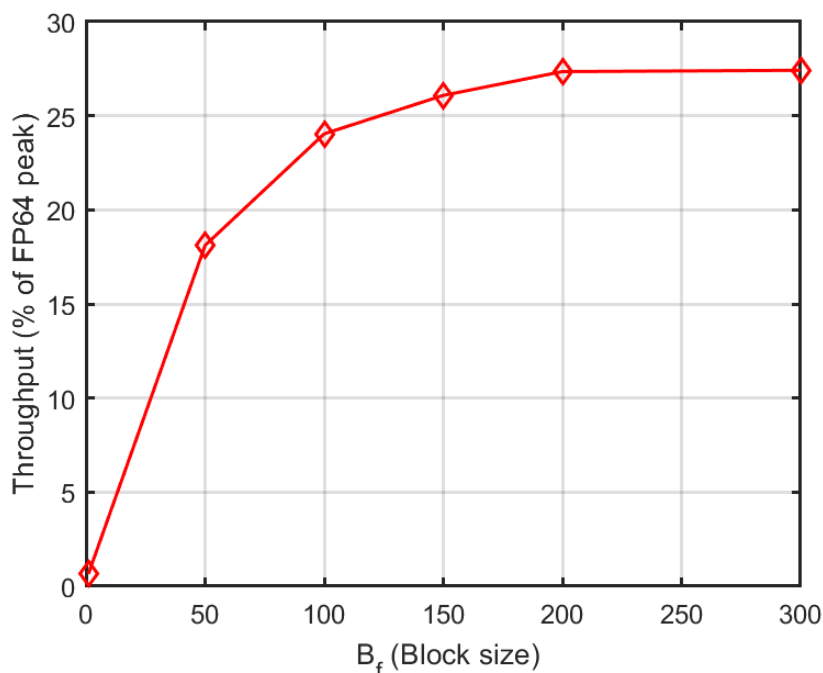


Fig: Chebyshev filtering throughput on 2 Summit nodes using 12 GPUs for various block sizes. FP64 peak of 2 Summit nodes is 87.6 TFLOPS

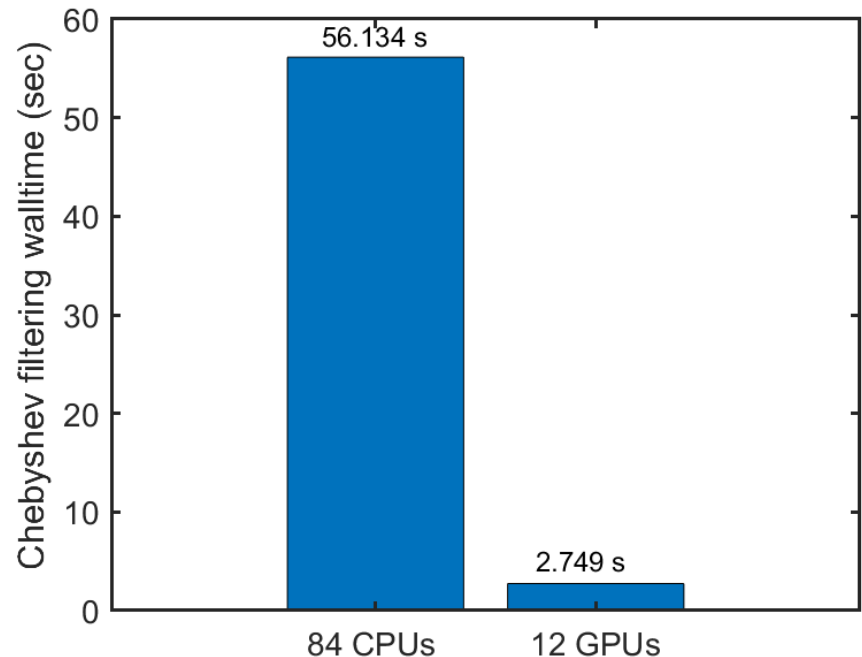
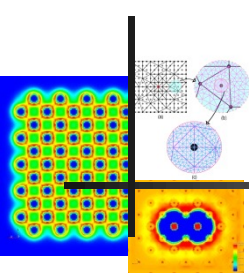


Fig: 20.4x GPU speed up for Chebyshev filtering. CPU run used 2 Summit nodes with 42 MPI tasks per node while GPU run used 2 Summit nodes with 12 GPUs





Orthogonalization: Cholesky Gram-Schmidt

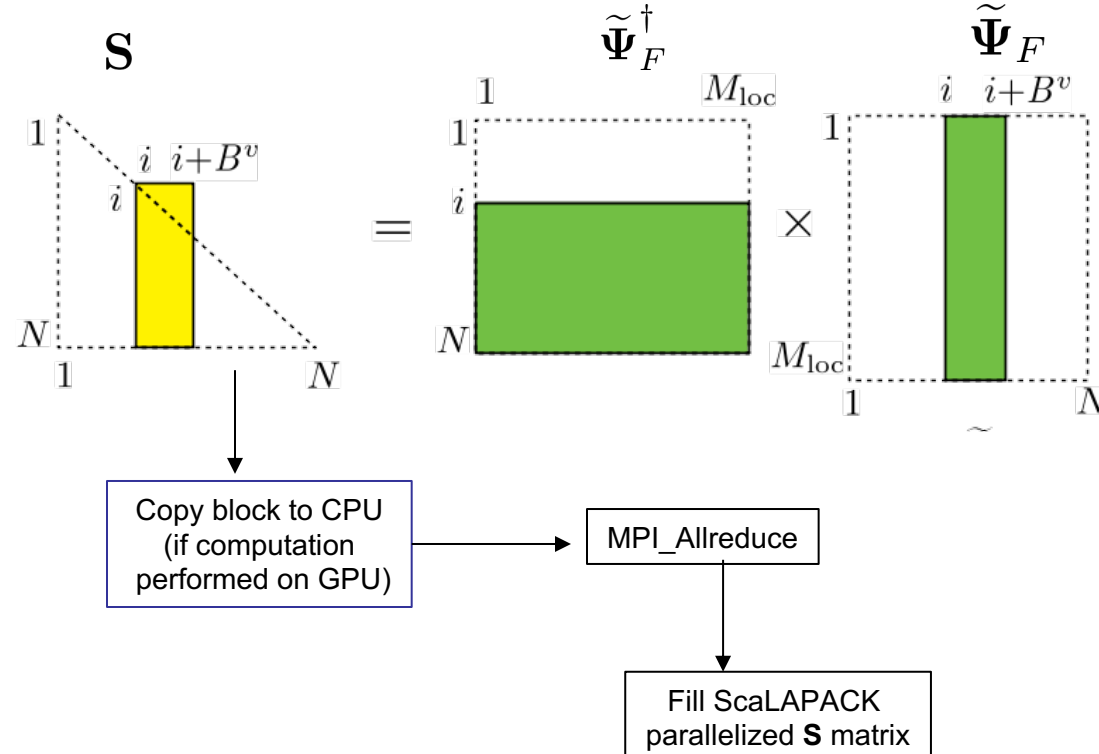
- Cholesky factorization of the overlap matrix: $\mathbf{S} = \tilde{\Psi}_F^\dagger \tilde{\Psi}_F = \mathbf{L}\mathbf{L}^\dagger. \mathcal{O}(MN^2)$
- Orthonormal basis construction: $\tilde{\Psi}_F^o = \tilde{\Psi}_F \mathbf{L}^{-1\dagger}. \mathcal{O}(MN^2)$

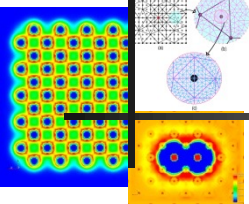
Mixed precision computation for Chol-GS

1. $\mathbf{S} = \text{DP } \{\mathbf{S}_d\} + \text{SP } \{\mathbf{S}_{od}\}$
2. $\mathbf{S} = \mathbf{L}\mathbf{L}^\dagger$ in double precision.
3. Orthonormal basis construction:

$$\tilde{\Psi}_F^o = \text{DP } \left\{ \tilde{\Psi}_F \mathbf{L}_d^{-1\dagger} \right\} + \text{SP } \left\{ \tilde{\Psi}_F \mathbf{L}_{od}^{-1\dagger} \right\}$$

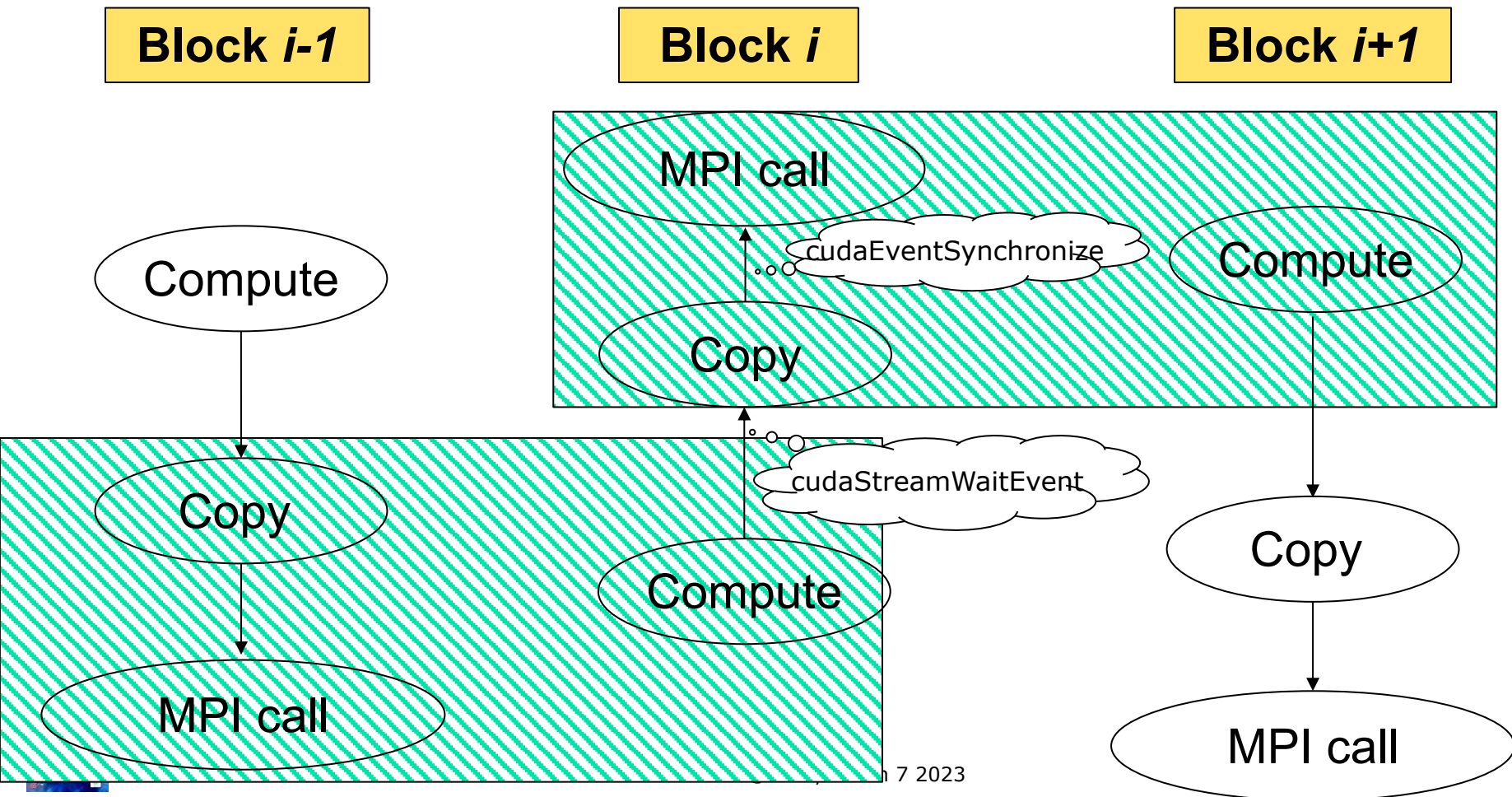
Blocked approach to reduce peak memory

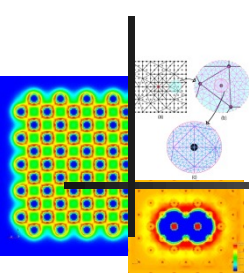




Overlapping compute and data movement on GPUs

Execute copy and MPI calls of current block asynchronously with compute of the successive block.



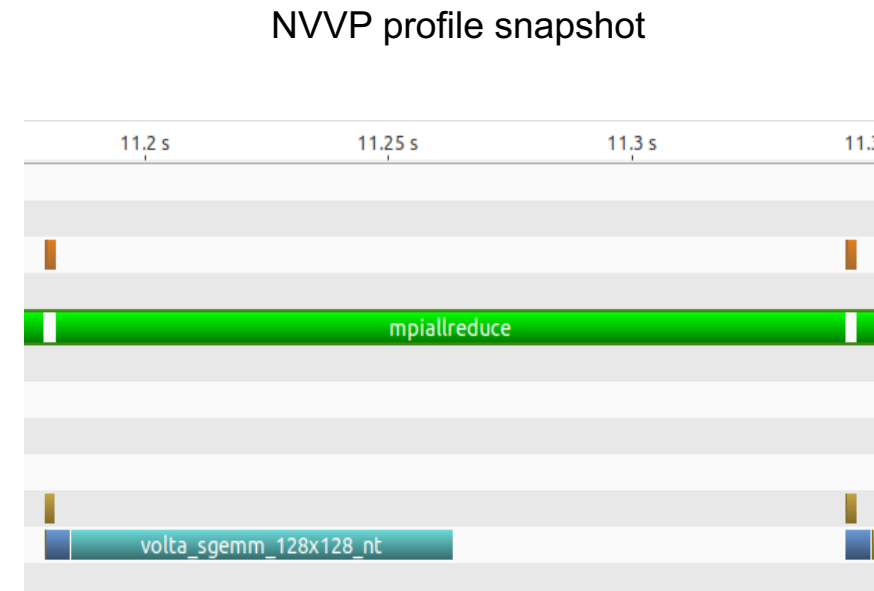
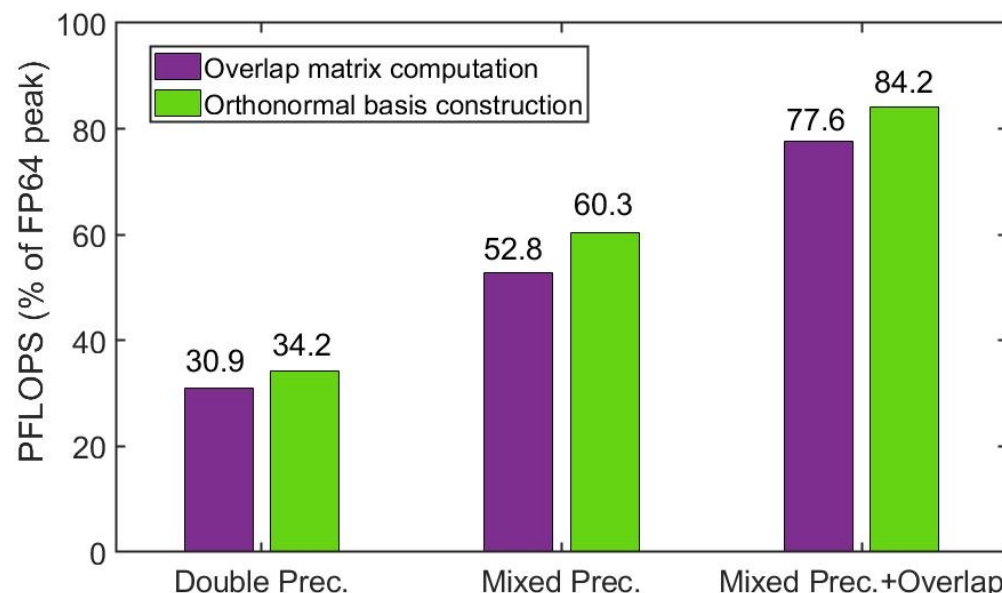


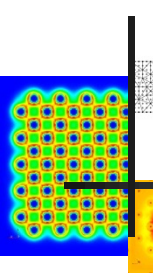
Orthogonalization: Cholesky Gram-Schmidt

Summit GPU cluster benchmark

Performance improvements due to mixed precision algorithm, and overlapping compute and data movement.

Case study: Mg dislocation system (61,640 electrons) using 1300 Summit nodes





Rayleigh-Ritz procedure

- Compute projected Hamiltonian: $\hat{\mathbf{H}} = \tilde{\Psi}_F^{\text{o}\dagger} \tilde{\mathbf{H}} \tilde{\Psi}_F^{\text{o}}$. $\mathcal{O}(MN^2)$
- Diagonalization of $\hat{\mathbf{H}}$: $\hat{\mathbf{H}}\mathbf{Q} = \mathbf{Q}\mathbf{D}$. $\mathcal{O}(N^3)$
- Subspace rotation step: $\tilde{\Psi}^{\text{R}} = \tilde{\Psi}_F^{\text{o}} \mathbf{Q}$. $\mathcal{O}(MN^2)$

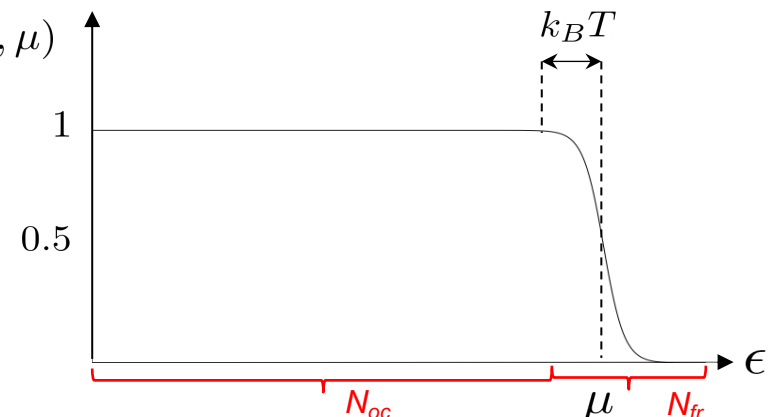
Mixed precision computation for RR

Compute projected Hamiltonian: $f(\epsilon, \mu)$

$$\rho_{\text{out}}^h(\mathbf{x}) = 2 \sum_{i=1}^N f(\epsilon_i^h, \mu) |\psi_i^h(\mathbf{x})|^2$$

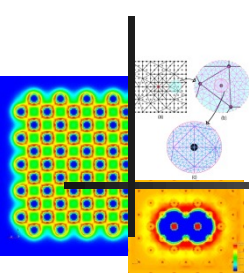
$$\tilde{\Psi}_F^{\text{o}} = \begin{bmatrix} \tilde{\Psi}_{\text{oc}}^{\text{o}} & \tilde{\Psi}_{\text{fr}}^{\text{o}} \end{bmatrix}$$

$$\left[\begin{array}{c|c} \hat{\mathbf{H}}_{\text{oc-oc}} & \hat{\mathbf{H}}_{\text{oc-fr}} \\ \hline \hat{\mathbf{H}}_{\text{fr-oc}} & \hat{\mathbf{H}}_{\text{fr-fr}} \end{array} \right] = \left[\begin{array}{c|c} \text{SP} \left\{ \tilde{\Psi}_{\text{oc}}^{\text{o}\dagger} \tilde{\mathbf{H}} \tilde{\Psi}_{\text{oc}}^{\text{o}} \right\} & \text{SP} \left\{ \tilde{\Psi}_{\text{oc}}^{\text{o}\dagger} \tilde{\mathbf{H}} \tilde{\Psi}_{\text{fr}}^{\text{o}} \right\} \\ \hline \text{SP} \left\{ \tilde{\Psi}_{\text{fr}}^{\text{o}\dagger} \tilde{\mathbf{H}} \tilde{\Psi}_{\text{oc}}^{\text{o}} \right\} & \text{DP} \left\{ \tilde{\Psi}_{\text{fr}}^{\text{o}\dagger} \tilde{\mathbf{H}} \tilde{\Psi}_{\text{fr}}^{\text{o}} \right\} \end{array} \right]$$



Subspace rotation step: $\tilde{\Psi}^{\text{R}} = \text{DP} \left[\tilde{\Psi}_F^{\text{o}} \mathbf{Q}_d \right] + \text{SP} \left[\tilde{\Psi}_F^{\text{o}} \mathbf{Q}_{od} \right]$



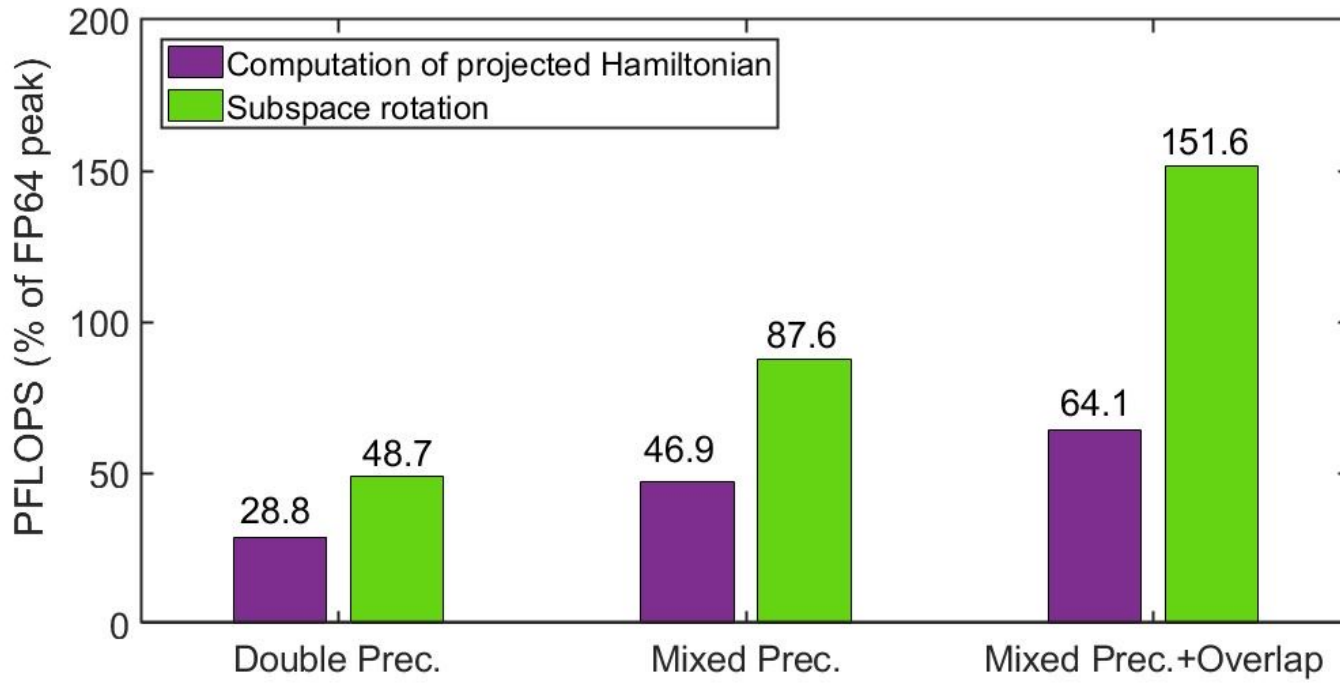


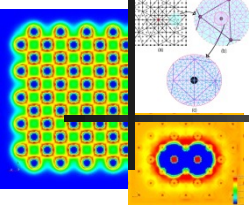
Rayleigh-Ritz procedure

- Blocked approach used for memory optimization
- Compute and communication are overlapped taking advantage of blocked approach.

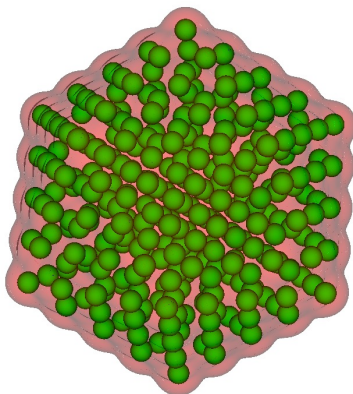
Summit GPU cluster benchmark

Case study: 61,640 electrons system using 1300 Summit nodes

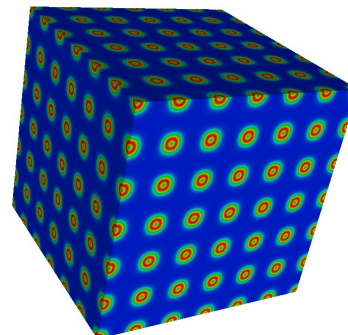




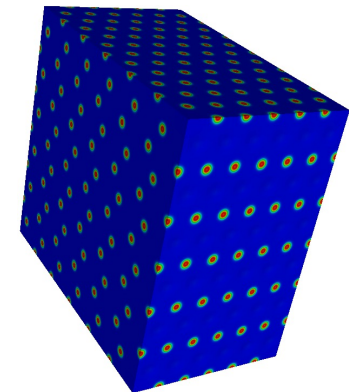
Accuracy and robustness of mixed precision computations



I. Cu nanoparticle
5871 electrons



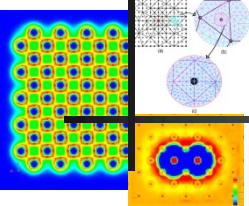
II. Mo periodic
supercell w/ vacancy
6034 electrons



III. Mg periodic
supercell w/ vacancy
8630 electrons

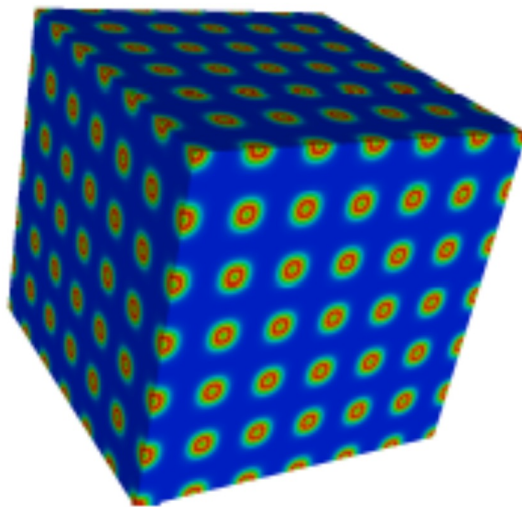
Energy error (Ha/atom)	5×10^{-12}	7×10^{-12}	3×10^{-12}
Max force error (Ha/Bohr)	3×10^{-6}	7×10^{-7}	2×10^{-6}
Total SCFs (DP, MP)	(46,46)	(30,30)	(18,18)





Comparison of DFT-FE & Quantum Espresso

- Vacancy in BCC Mo – periodic calculation ; ONCV pseudopotential
- Accuracy for all calculations $<0.1\text{mHa/atom}$ ($\sim 2\text{meV/atom}$)

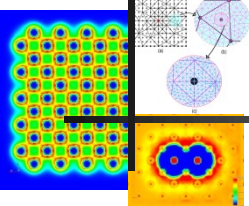


BCCMo $6 \times 6 \times 6$ monovacancy
(6034 electrons)

Compute resources per SCF in Node-Hrs
(NERSC Cori KNL)

System size	Quantum-ESPRESSO (Ecut: 20 Ha)	DFT-FE (h_min: 2.1, p=7)
431 atoms (N _e = 6034)	0.56	0.24
1023 atoms (N _e = 14322)	22.1	1.4
1999 atoms (N _e = 27986)	219.5	7.5



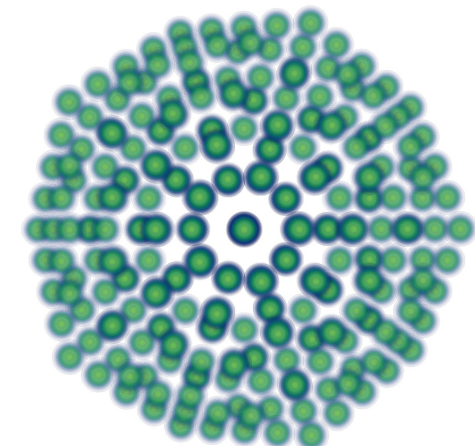


Comparison of DFT-FE & Quantum Espresso

- Cu nanoparticles; ONCV pseudopotential
- Accuracy for all calculations $<0.1\text{mHa/atom}$ ($\sim 2\text{meV/atom}$)

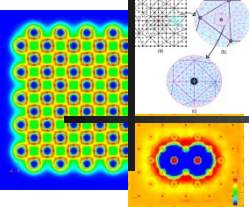
Compute resources per SCF in Node-Hrs
(NERSC Cori KNL)

System size	Quantum-ESPRESSO (Ecut: 50 Ha)	DFT-FE (h_min: 0.8; p=6)
147 atoms (N _e = 2793)	0.2	0.22
309 atoms (N _e = 5871)	5.5	1.3
561 atoms (N _e = 10569)	63.4	4.2
923 atoms (N _e = 17537)	-	10.9



Cu4shell (5871 electrons)

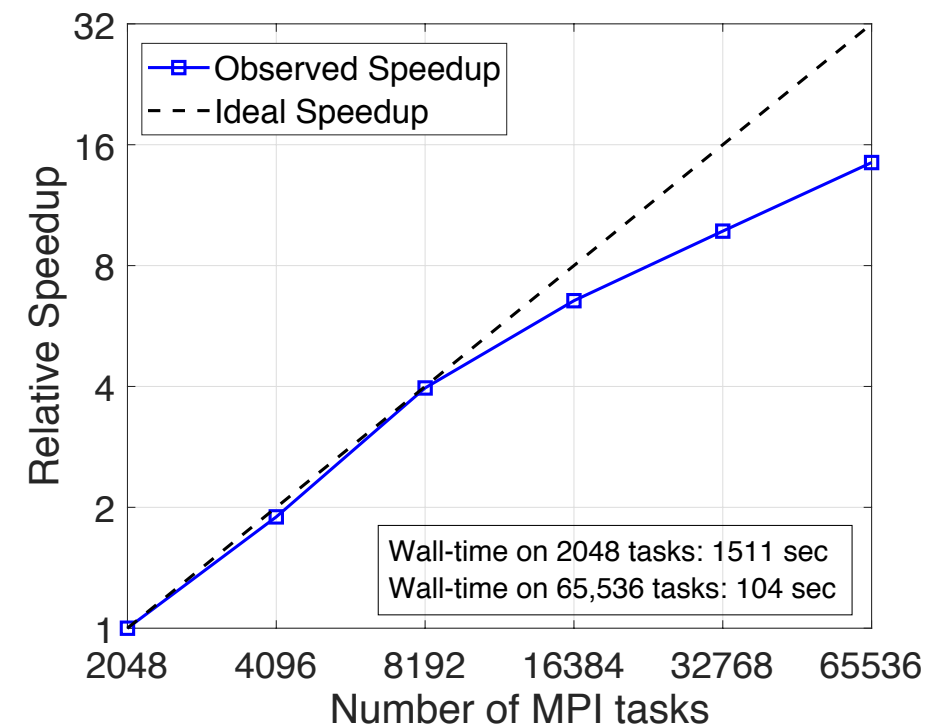




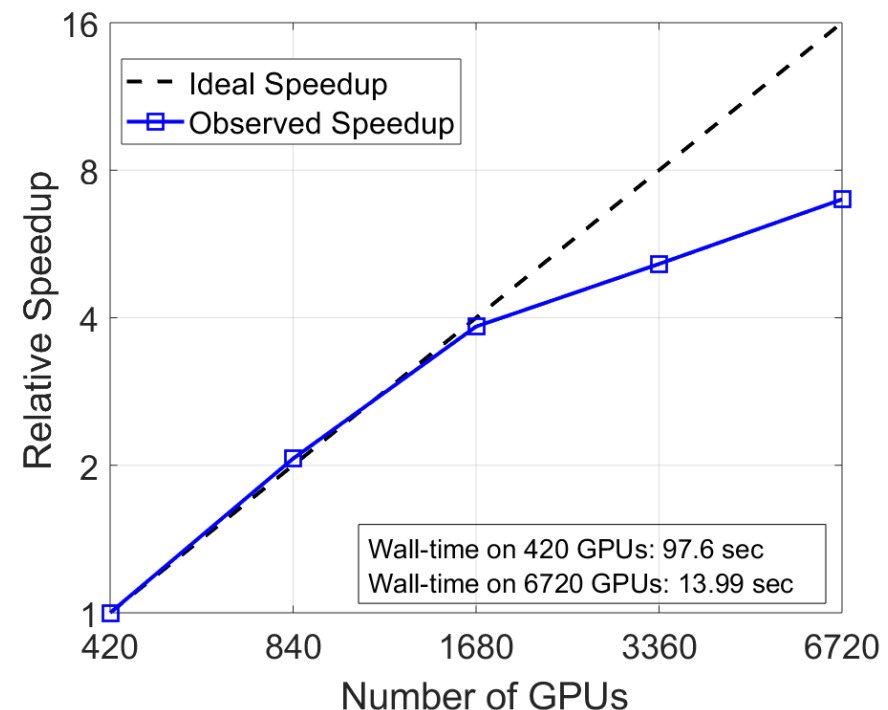
Strong Scaling & Time to solution

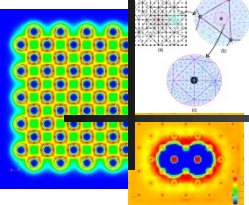
Mg pyr II screw dislocation – 1,848 atoms (18,480 e⁻); 55.11 million FE DoFs

Theta (ALCF)



Summit GPUs (OLCF)

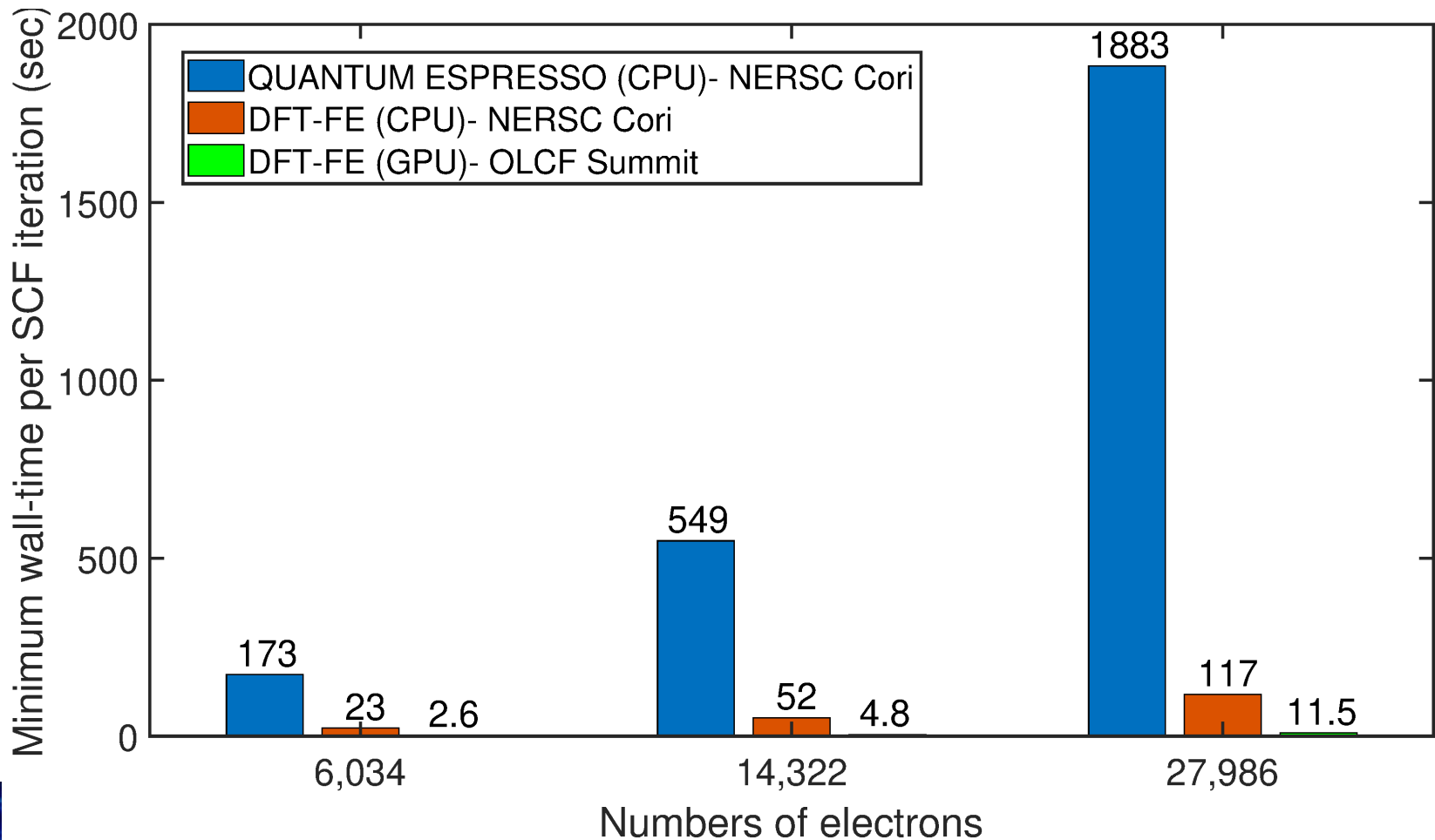


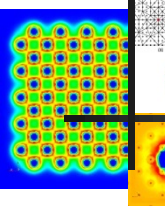


Minimum wall-time comparison with plane-wave basis

Vacancy in Mo – periodic calculation ; ONCV pseudopotential

Accuracy for all calculations <0.1mHa/atom (\sim 2meV/atom)





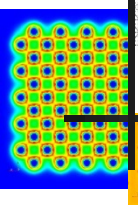
DFT-FE – Open source code

(<https://github.com/dftfeDevelopers/dftfe>;

Motamarri et al. Comput. Phys. Commun. (2020); Das et al. Comput. Phys. Commun. (2022))

- Discretization: FE basis; adaptive mesh refinement
- Geometry: Periodic, non-periodic, semi-periodic
- Physics:
 - ❖ Pseudopotential (TM; ONCV) and All-electron calculations (classical FE)
 - ❖ Density based XC functionals
- Calculations:
 - ❖ Ground-state energy
 - ❖ Geometry (ionic and cell) relaxation (Motamarri & Gavini, Phys. Rev. B 97, 165132 (2018))
 - ❖ Ab-initio MD
- Scaling: Tested on Summit, Theta, Stampede, Comet, Cori (up 192,000 cores)
- System sizes: 100,000 electron pseudopotential calculations; 10,000 electron all-electron calculations
- Ported to GPUs:
 - ❖ ~20x speedups (on Summit) in comparison to CPUs on a node-to-node basis
 - ❖ 64PLOPS of sustained performance; ~38% efficiency on Summit
 - ❖ Finalist, 2019 Gordon Bell prize





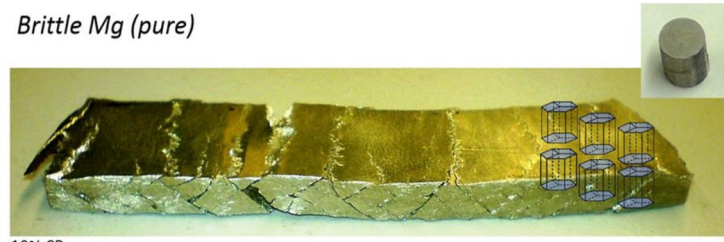
Application I: Technological challenge of low ductility in Mg

- Magnesium is the lightest structural metal with high strength to weight ratio
 - ❖ 75% lighter than Steel and 30% lighter than Aluminum
- Every 10% reduction in the weight of a vehicle will result in 6-8% increase in fuel efficiency.
 - ❖ Important implications to fuel efficiency and reducing carbon footprint
- Low ductility key issue in the manufacturability of structural components. Main limitation in the adoptability of Mg and Mg alloys in automotive and aerospace sectors. (T.M. Pollock, *Science* **328**, 986-987 (2010))



Courtesy: <https://www.audi-technology-portal.de/en/body>
Current state of art: Hybrid Steel and Aluminum construction

Brittle Mg (pure)

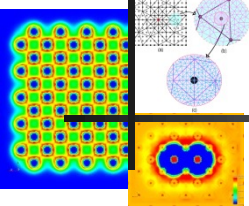


10% CR

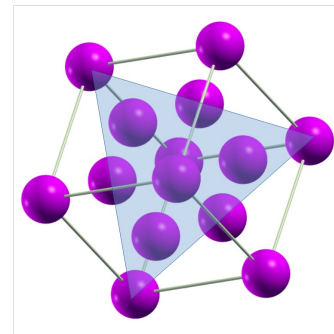
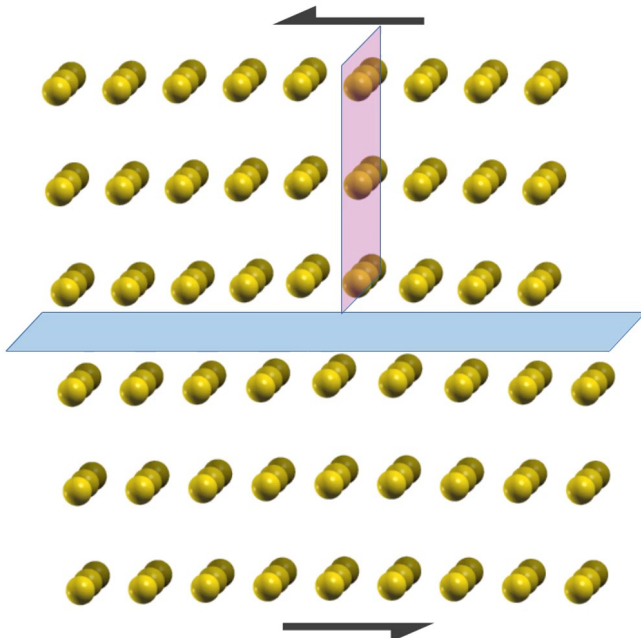
CR: cold rolled

S. Sandlöbes et al. Scientific Reports 7, 10458 (2017).



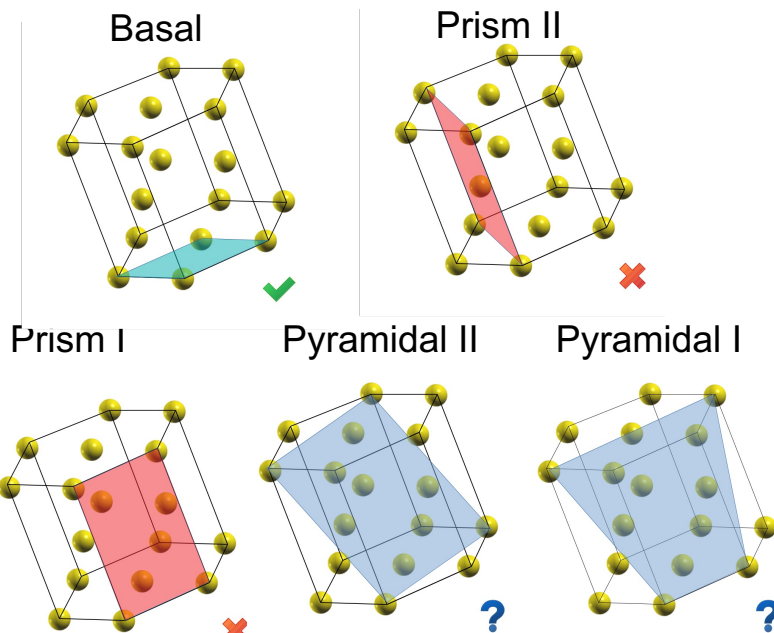


Technological challenge of low ductility in Mg

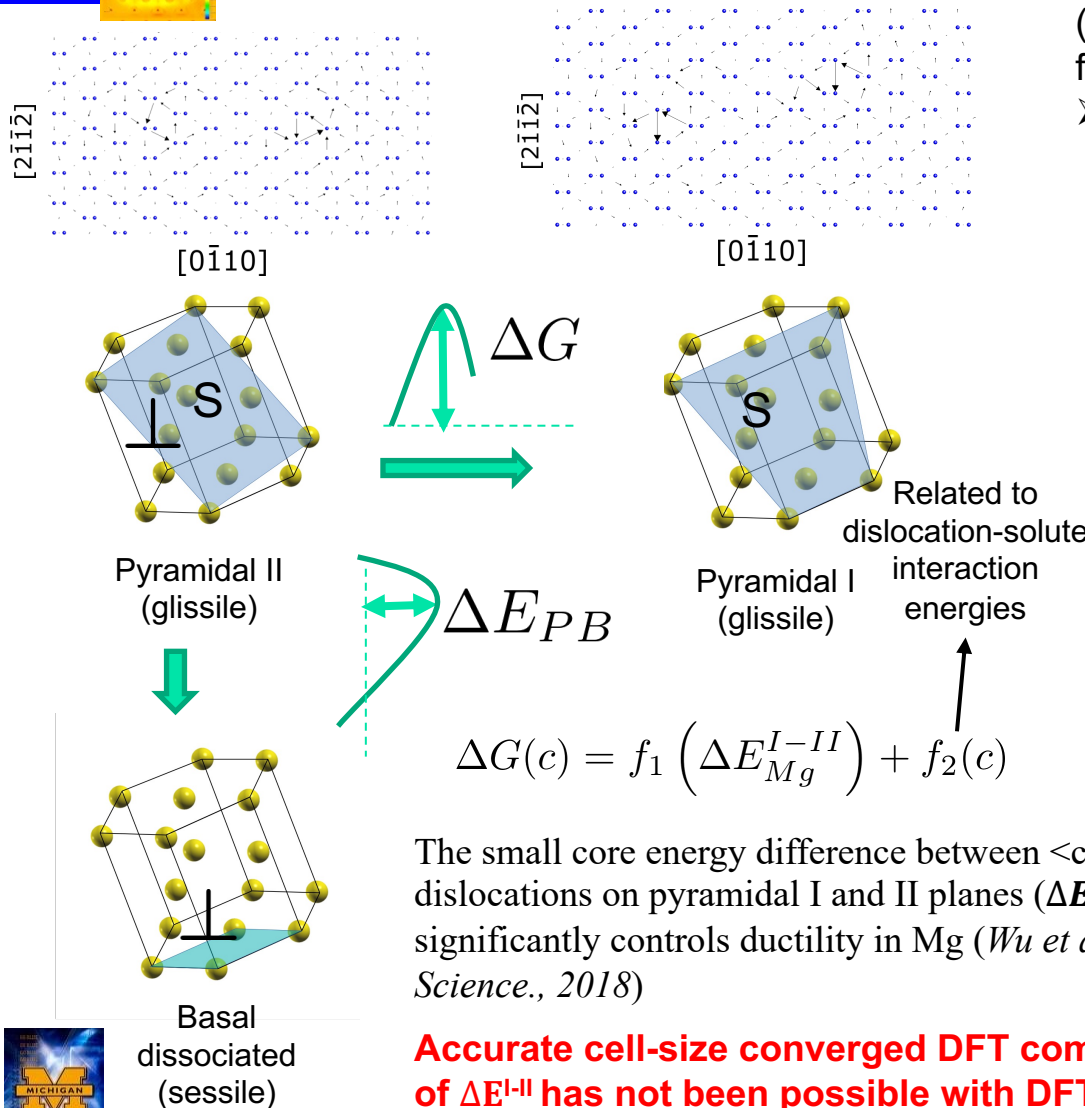
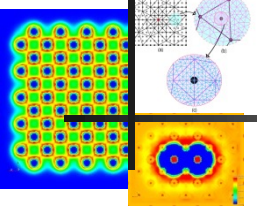


12 slip systems in Face Centered Cubic Crystals → higher ductility

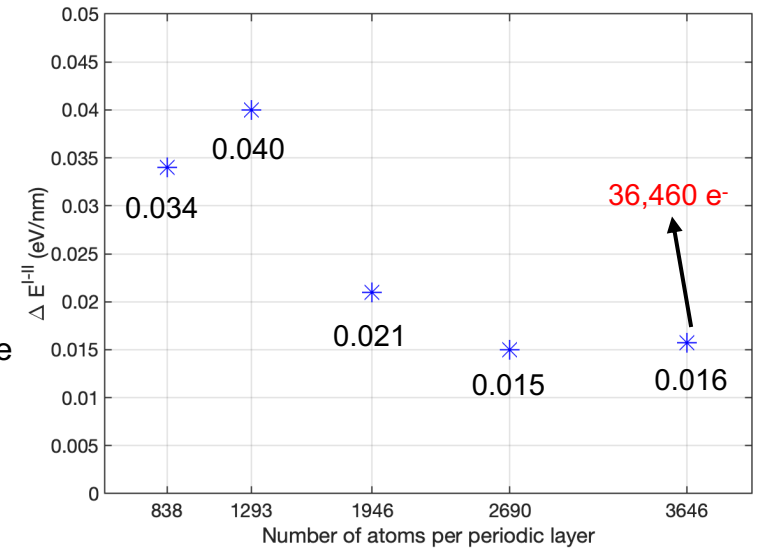
- ❖ Dislocations are energetically more favorable to reside on certain slip systems. (**Energetics**)
- ❖ Dislocation glide occurs after the applied shear stress is greater than the Perils barrier. (**Activation barrier**)
- ❖ More the number of slip systems where dislocations can glide easily higher is the ductility.



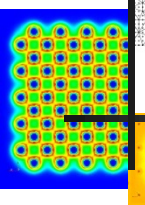
Accurate $\langle c+a \rangle$ dislocation core energetics for ductility enhancement in dilute Magnesium alloys



- Chemical accuracy for all calculations (<0.1mHa/atom energy and <0.1mHa/Bohr in forces)
- 12 k-points along the dislocation line



Uniaxial Strains	Slope (eV/nm)
ε_{11}	-1.450
ε_{22}	-3.507
ε_{33}	0.301



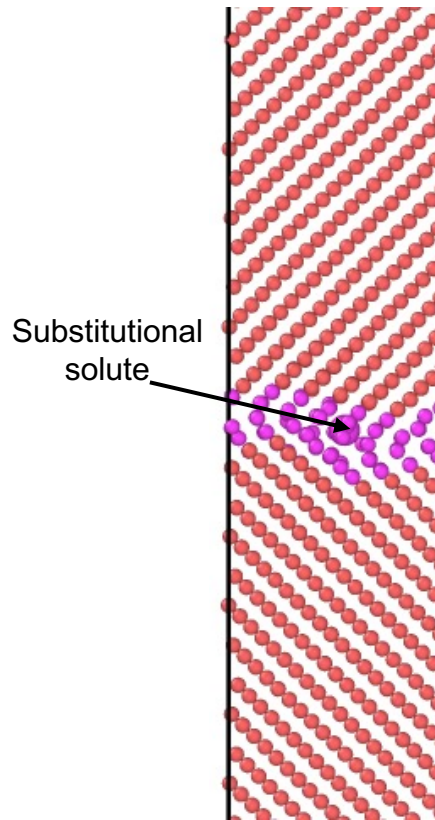
Solute grain boundary (GB) segregation energies in Magnesium

➤ GB solute segregation can enhance non-basal textures in Magnesium through solute drag effects (*Robson 2014, 2016 Met. Mat. Trans. A*)

➤ Understanding equilibrium segregation behavior, which is controlled by ΔE_{seg} , for different GB structures and different solute types with strong chemical interactions

➤ Use DFT computed segregation energies and transport coefficients to predict solute drag on GB

➤ **Challenge: DFT simulations of random GB geometries reaching 4000-5000 atoms with structural relaxation has remained infeasible.**



- Random grain boundary:
- ❖ Tilt axis: [1̄100]
 - ❖ Tilt angle: 44°
 - ❖ 1932 atoms

E_{GB} Energy with solute atom at a GB site

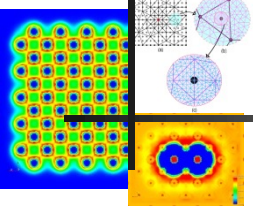
E_{bulk} Energy with solute atom away from GB

$$\Delta E_{seg} = E_{GB} - E_{bulk}$$

Solute type	ΔE_{seg} (eV)
Al (non-RE)	-0.109
Y (RE)	-0.320

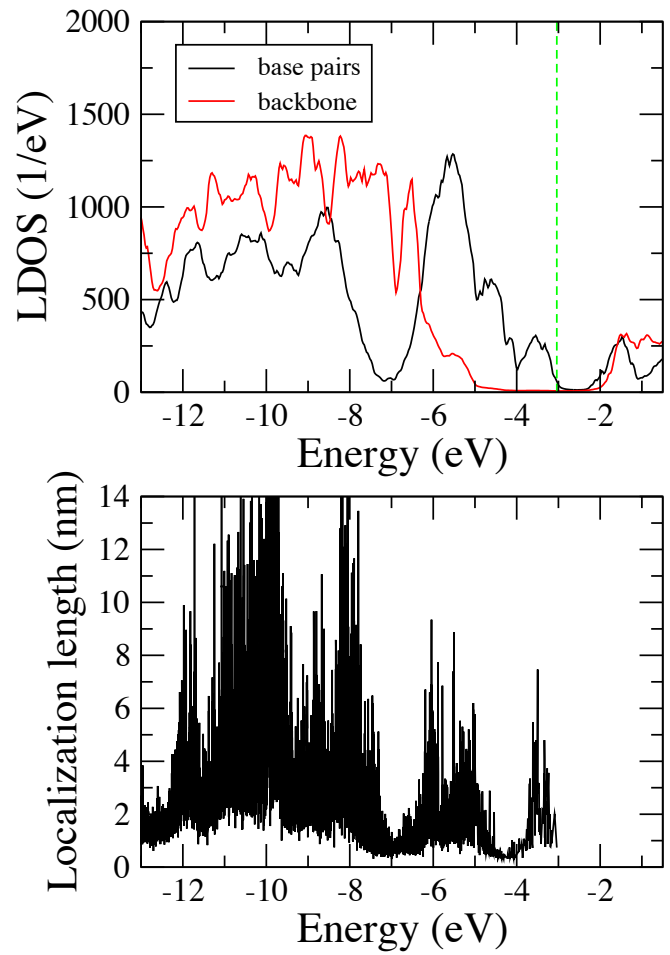
Calculations on larger GB systems with ~4000 atoms ongoing

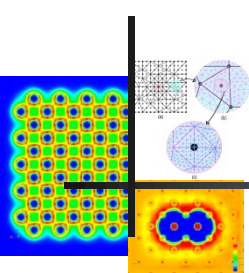




Other Application Studies using DFT-FE

- Understanding electron transport in DNA molecules (*Nature Nanotechnology* 15 836 (2020))
 - ❖ Large-scale simulations involving 100 basis pairs (~6,200 atoms) simulating experiments
 - ❖ Provided new insights into the role of backbone in electron charge transport
- Spin-spin interactions in defects in solids (*npj Computational Materials*, 50 (2021); *Phys. Rev. Mat.* 3 043801 (2019))
 - ❖ Computed spin Hamiltonian parameters that describe electron-electron and electron-nuclear spin interactions
 - ❖ Systematically convergent calculations with all-electron accuracy, possible for the first time
 - ❖ Use mixed pseudopotential and all-electron calculations leveraging the flexibility of the DFT-FE framework

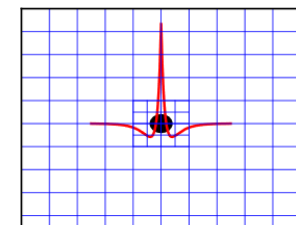
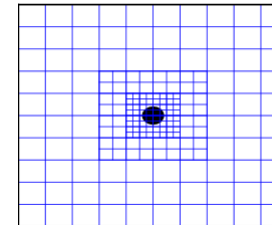
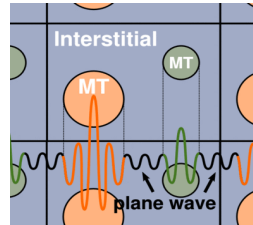
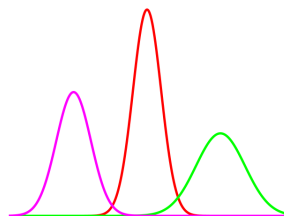


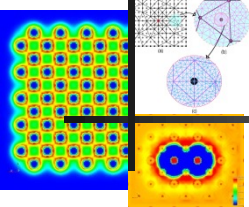


All-electron calculations

- More stringent basis set requirement to capture the fast oscillations of core electrons
- Need solving for all electrons; though some other approximations to avoid explicit computations can be used.

	Gaussian	APW/LAPW	Classical FE	Enriched FE
Convergence	☒ Incomplete basis, No systematic convergence	☑ Complete basis, Systematic convergence	☑ Complete basis, Systematic convergence	☑ Complete basis, Systematic convergence
Boundary Conditions	☒ using mixed BCs not easy	☒ Only handles periodic BCs	☑ Can handle all BCs	☑ Can handle all BCs
Parallel Scalability	☒ Non-local basis, Poor scalability	☒ Use of FFTs, Poor scalability	☑ Local basis, Good scalability	☑ Local basis, Good scalability
Robustness	☒ Ill-conditioned for large systems.	☒ Sensitive to energy parameters	☑ Well Conditioned	☑ Well Conditioned
Efficiency	☑ 10-100 basis/atom	☑ 100-1000 basis/atom	☒ $10^5 - 10^6$ basis/atom	☑ 10000-50000 basis/atom



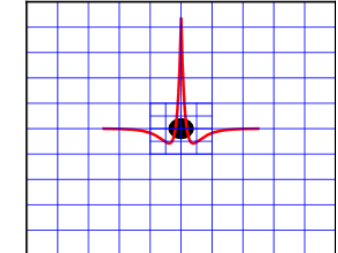


Enriched finite element basis

(Kanungo & Gavini, Phys Rev. B 95 035112 (2017); Rufus, Kanungo & Gavini Phys Rev. B 106 085112 (2021))

- Additional functions appended to the ‘Classical’ FE basis

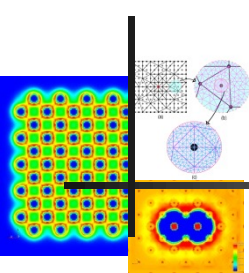
$$\psi^h(\mathbf{x}) = \sum_j N_j^C(\mathbf{x})\psi_j^C + \sum_k N_k^E(\mathbf{x})\psi_j^E$$



(Yamaka & Hodo PRB (2005); Sukumar & Pask IJNME (2009), Extreme Mech. Let. (2017))

- Enriched functions: Radial part computed using 1D radial Kohn-Sham solve, and multiplied by spherical harmonics
 - ❖ Compact support for the enriched functions is obtained by multiplying with a mollifier
- Orthogonalized enrichment: Orthogonalize with respect to the classical FE basis; improves conditioning of the basis
- Integrals computed using an adaptive quadrature (Mousavi et al. (2012))
- Key advantages of enrichment:
 - ❖ Reduced degrees of freedom
 - ❖ Reduced spectral width of the discrete Hamiltonian (especially important for Chebyshev filtering approach for solving the Kohn-Sham problem)

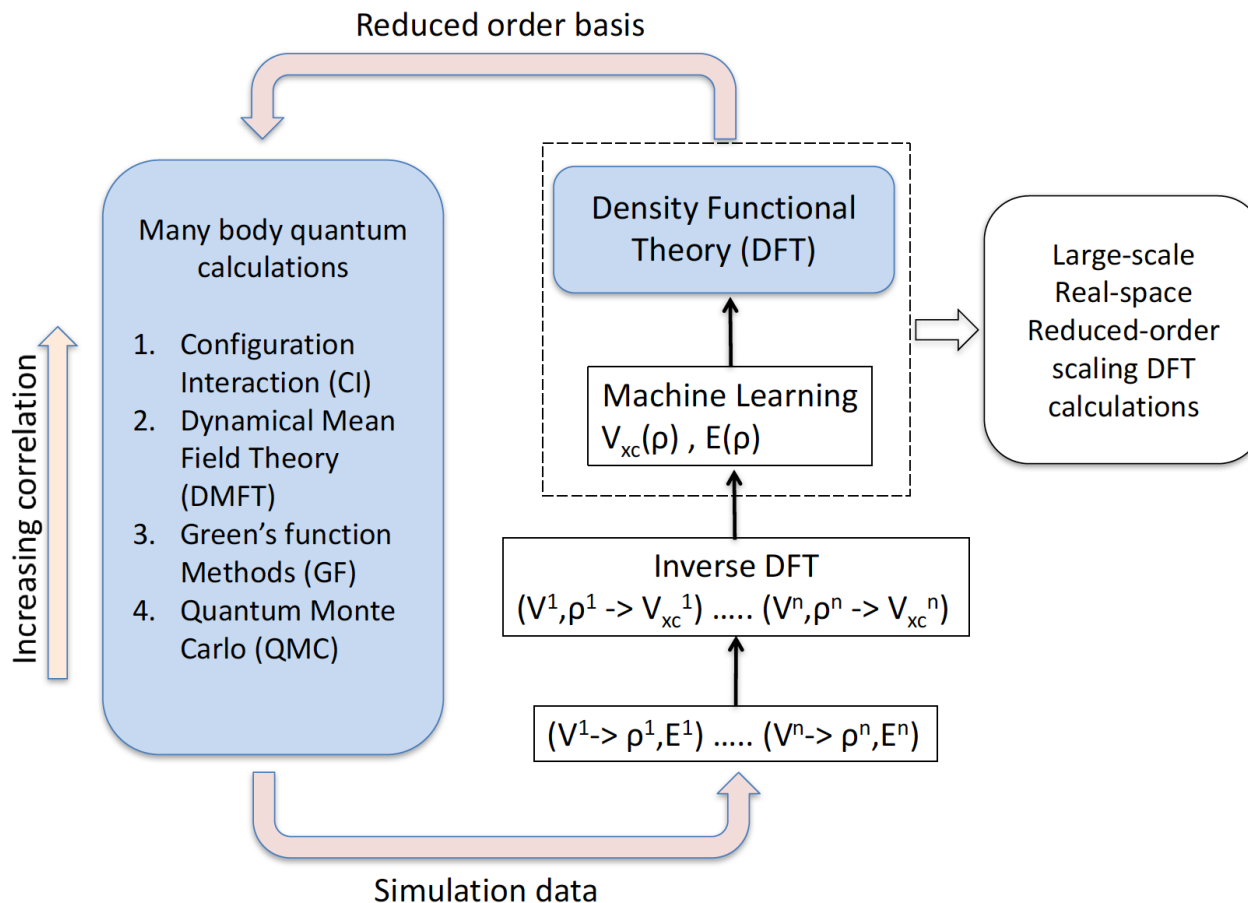




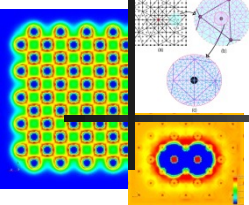
Large-scale quantum accuracy calculations

- Accuracy of exchange correlation functionals in DFT is not satisfactory for strongly correlated electrons.

Can we address this without sacrificing the efficiency of DFT calculations?



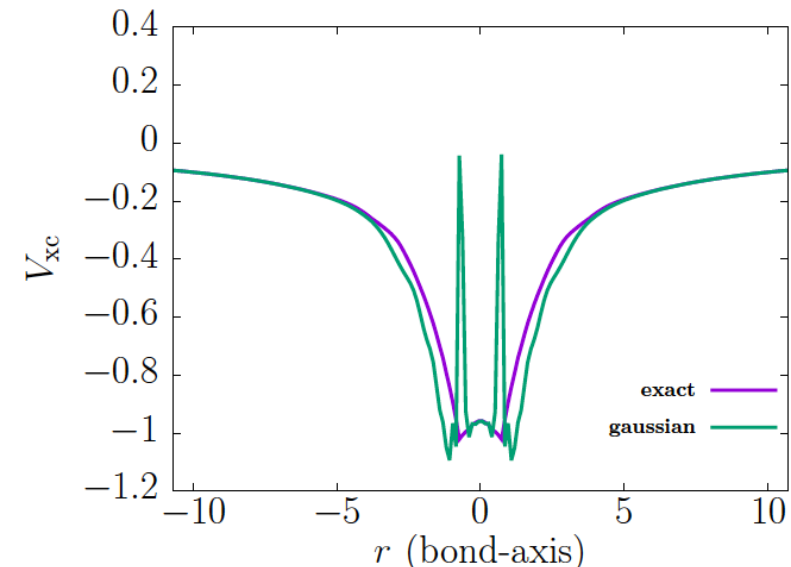
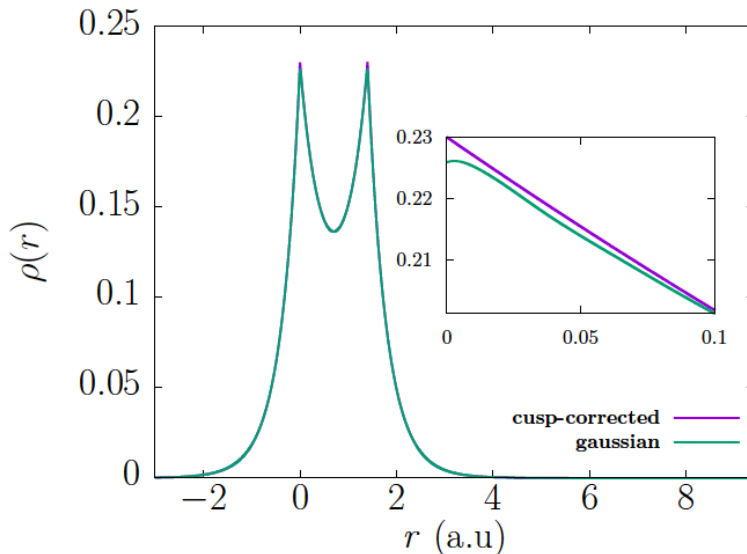
Inverse DFT

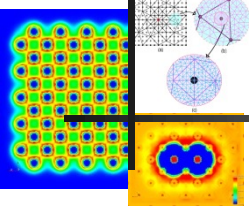


Inverse DFT: Determining $V_{xc}(\mathbf{r})$ given $\rho(\mathbf{r})$

Remained an open problem for 25 years – Numerically very challenging:

- Attempts included iterative approaches, constrained optimization approaches
 - ❖ Spurious oscillations; non-unique solutions
 - ❖ Key issues:
 - (i) Many-body QM calculations conducted in incomplete basis (wrong asymptotics)
 - (ii) Inversion in an incomplete basis





Inverse DFT

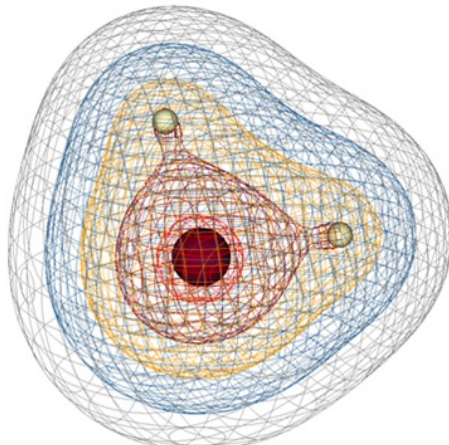
(Kanungo, Zimmerman & Gavini, Nature Communications **10** 4497 (2019))

Recent breakthrough in an accurate solution to the inverse DFT problem.
Demonstrated on molecular systems that are both weakly and strongly correlated.

$$\Psi(\mathbf{r}_1, \mathbf{r}_2, \dots, \mathbf{r}_{N_e})$$

Many-body wavefunction

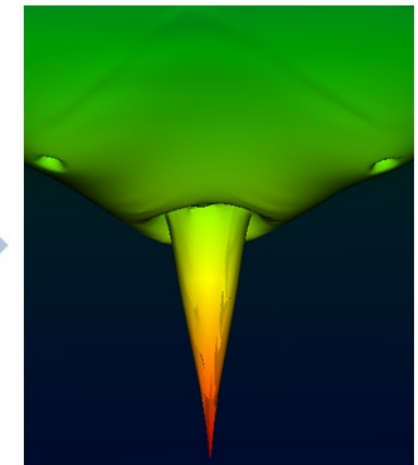
Configuration
Interaction

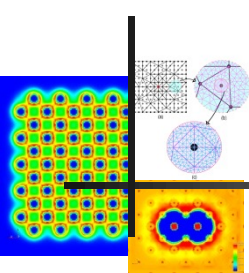


$$\rho(\mathbf{r}) \xleftrightarrow{v_{xc}[\rho(\mathbf{r})]} v_{xc}(\mathbf{r})$$

*Inverse
DFT*

- ❖ PDE-Constrained Optimization
- ❖ Complete Finite-element basis
- ❖ Cusp Correction
- ❖ Correct Asymptotics





Inverse DFT – Key Ideas

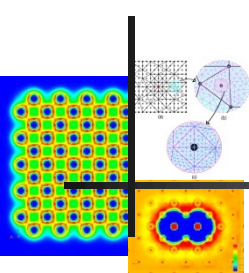
- PDE constrained optimization

$$\arg \min_{v_{xc}(\mathbf{r})} \int w(\mathbf{r}) (\rho_{data}(\mathbf{r}) - \rho(\mathbf{r}))^2 d\mathbf{r}$$

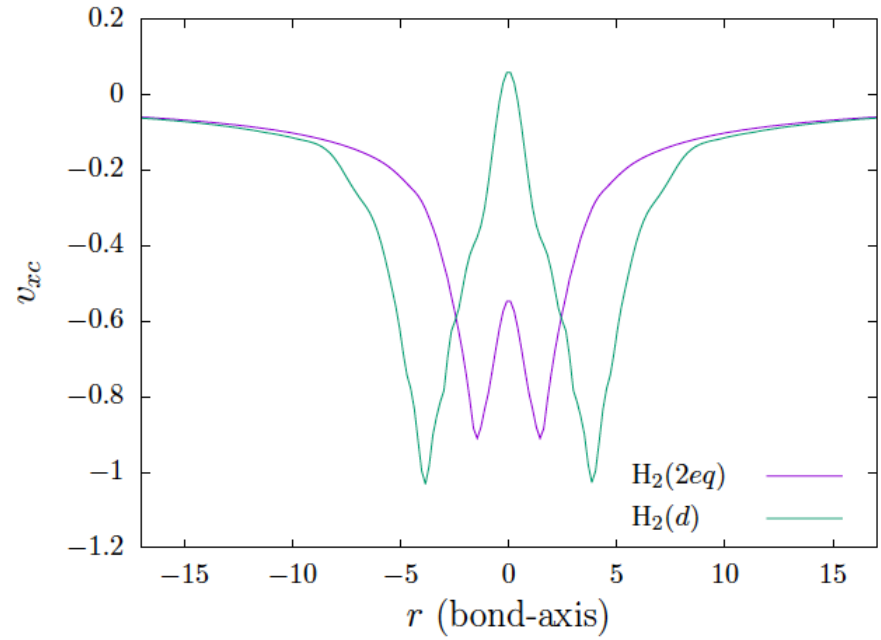
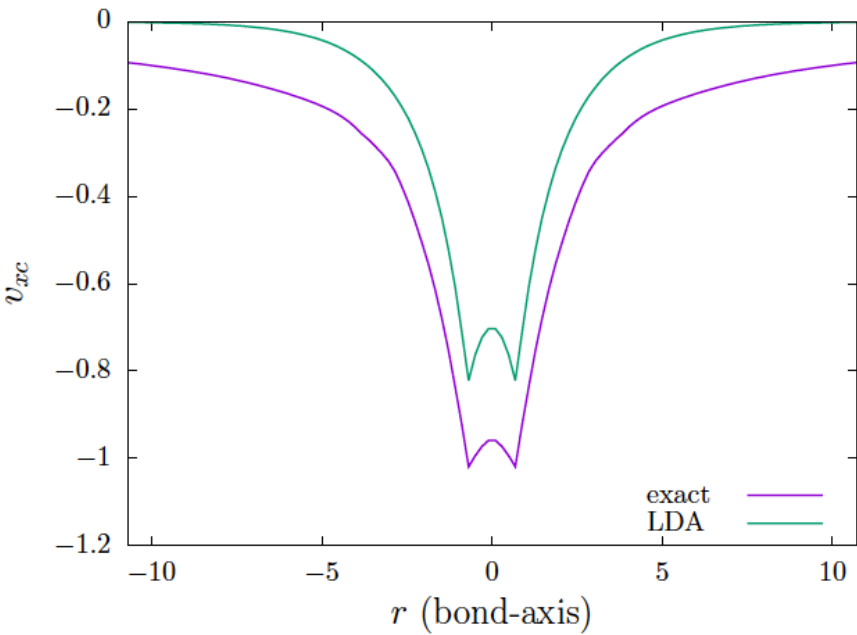
subject to

$$\left(-\frac{1}{2} \nabla^2 + v_{\text{ext}}(\mathbf{r}) + v_{\text{H}}(\mathbf{r}) + v_{\text{xc}}(\mathbf{r}) \right) \psi_i = \epsilon_i \psi_i, \quad \int |\psi_i(\mathbf{r})|^2 d\mathbf{r} = 1.$$

- Higher-order FE basis for discretization – ensures completeness
- Cusp correction: $\Delta\rho(\mathbf{r}) = \rho_{FE}^{DFT}(\mathbf{r}) - \rho_G^{DFT}(\mathbf{r})$
- Far-field asymptotics: Start with a guess for $V_{xc}(\mathbf{r})$ with correct far-field asymptotics and use homogeneous Dirichlet boundary conditions on the adjoint fields.

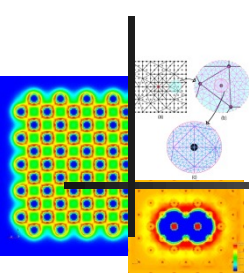


Inverse DFT using ab-initio correlated densities



Good agreement between HOMO eigenvalue and $-I_p$



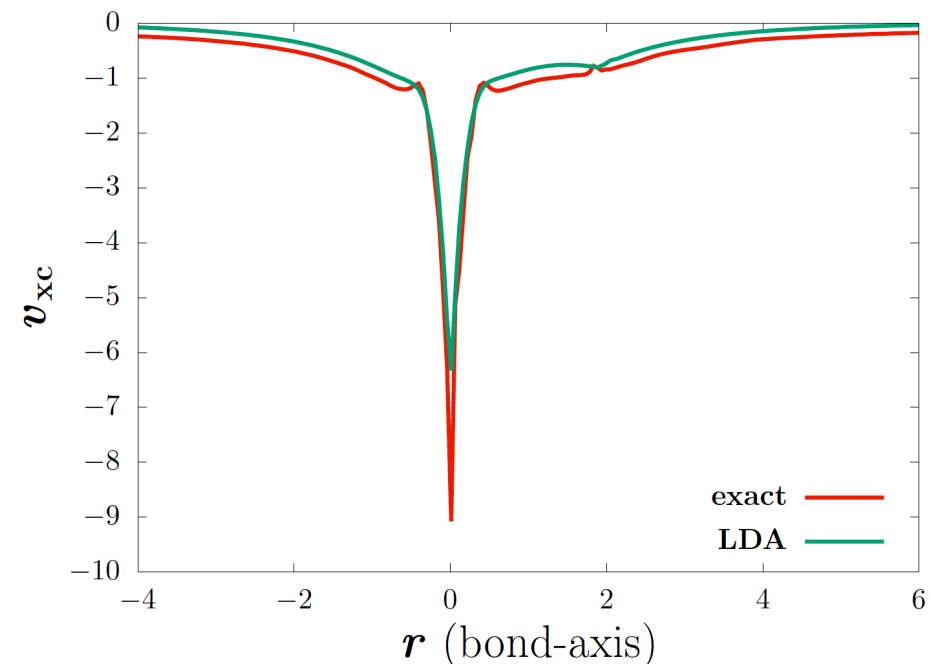
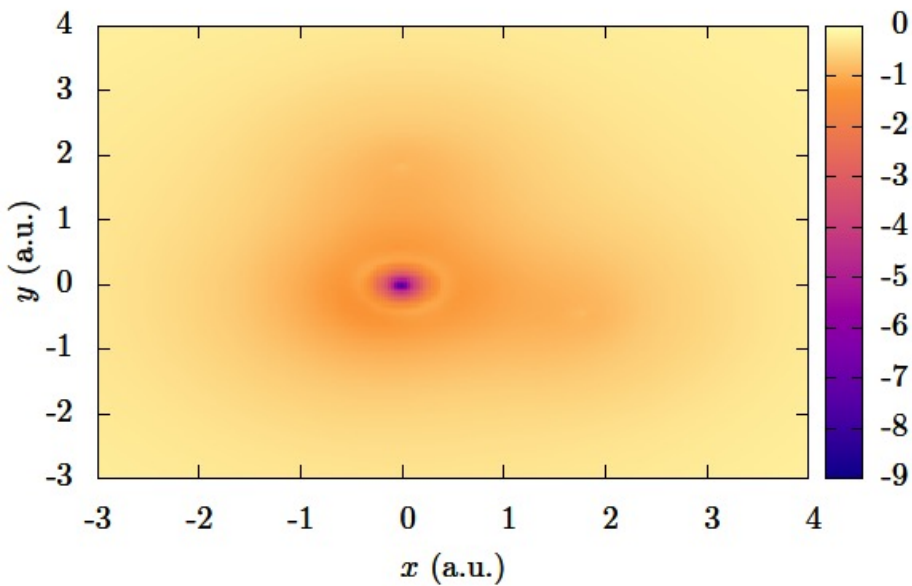


Inverse DFT using ab-initio correlated densities

Materials system H_2O molecule

Exact V_{xc}

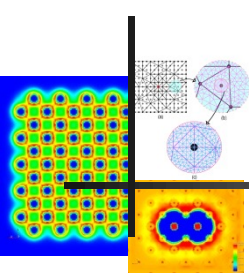
(data from full CI calculation)



Verification of Koopmans' theorem:

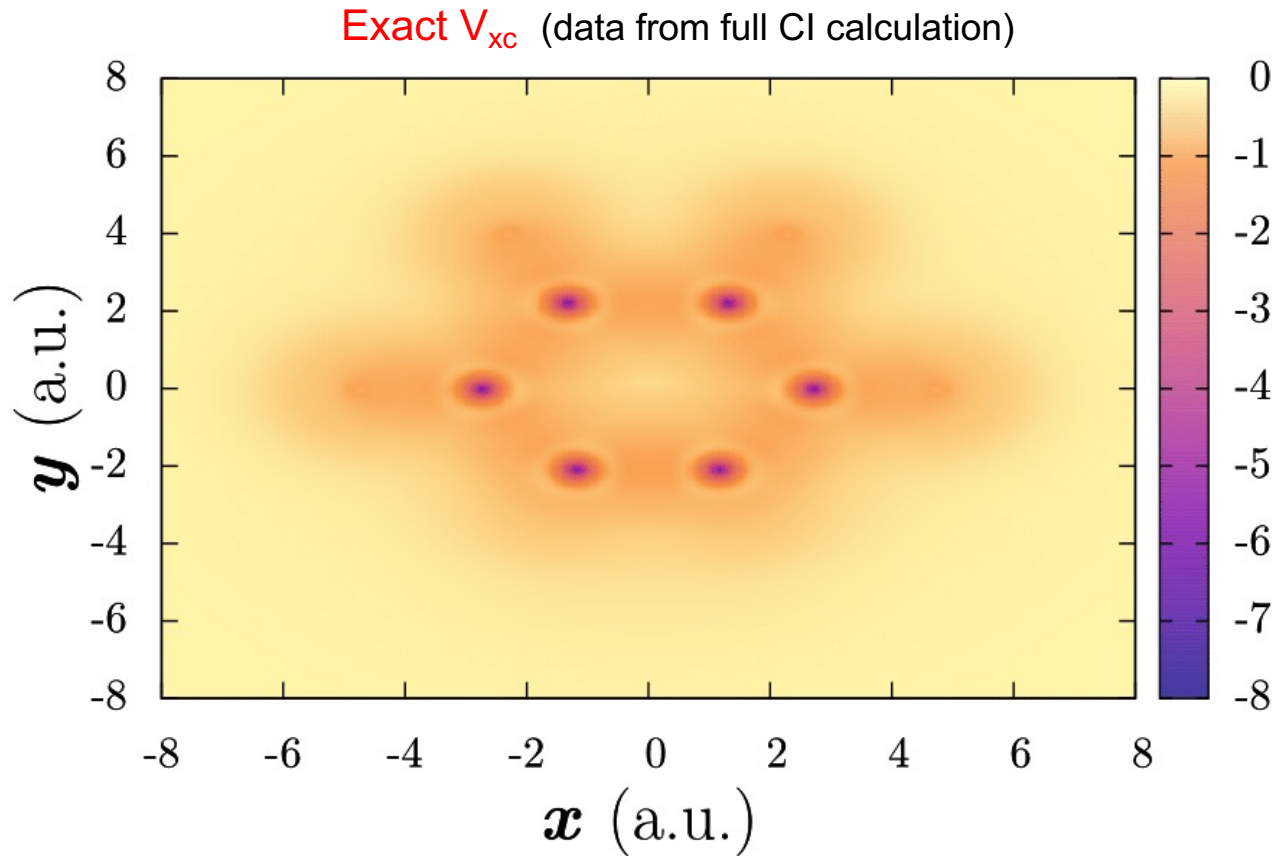
HOMO eigenvalue = -0.452 Ha; $-I_p = -0.454$ Ha





Inverse DFT using ab-initio correlated densities

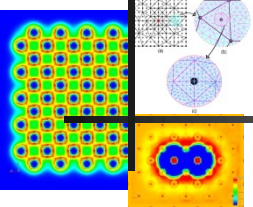
Materials system C_6H_4 (*ortho*-Benzene) – strongly correlated system



Verification of Koopmans' theorem:

HOMO eigenvalue = -0.354 Ha; $-I_p = -0.355$ Ha

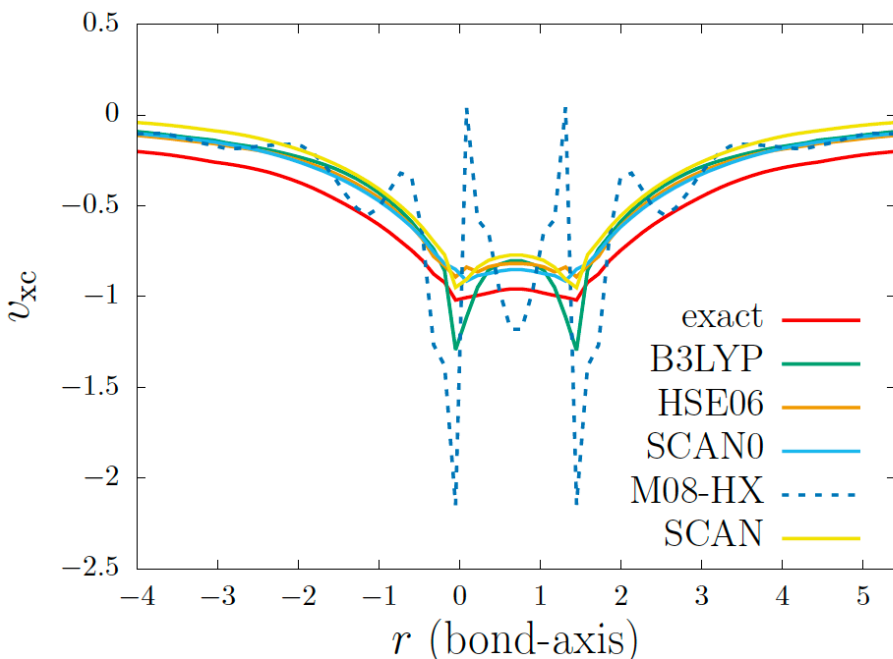




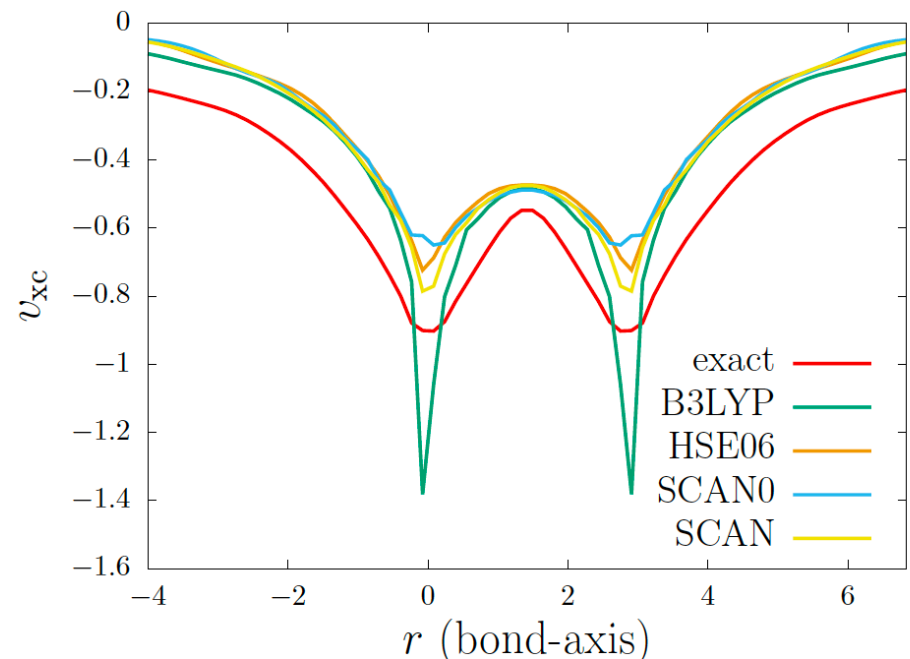
Comparison of exact XC with model XC potentials

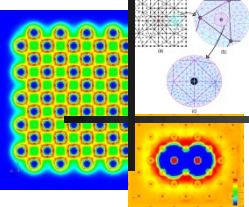
(Kanungo, Zimmerman & Gavini, J. Phys. Chem. Lett. **12** 12012 (2021))

H_2 – equilibrium bond length

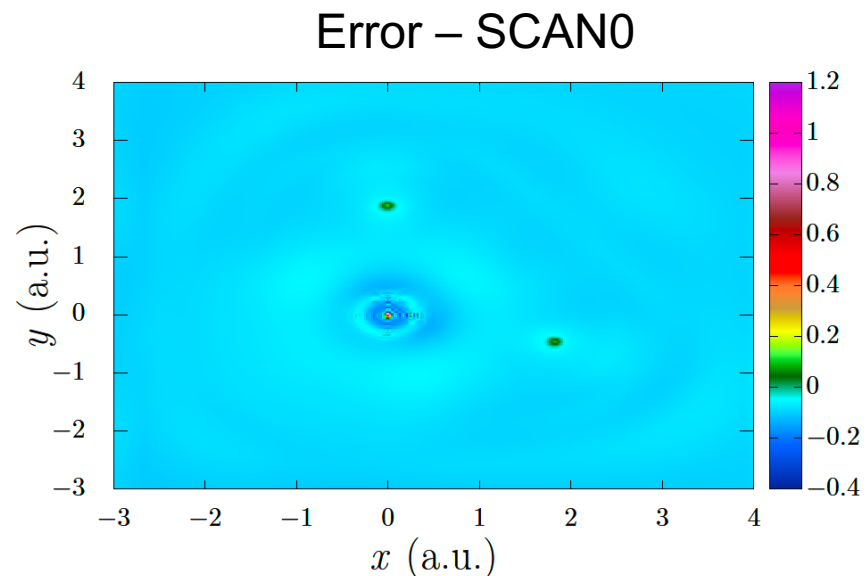
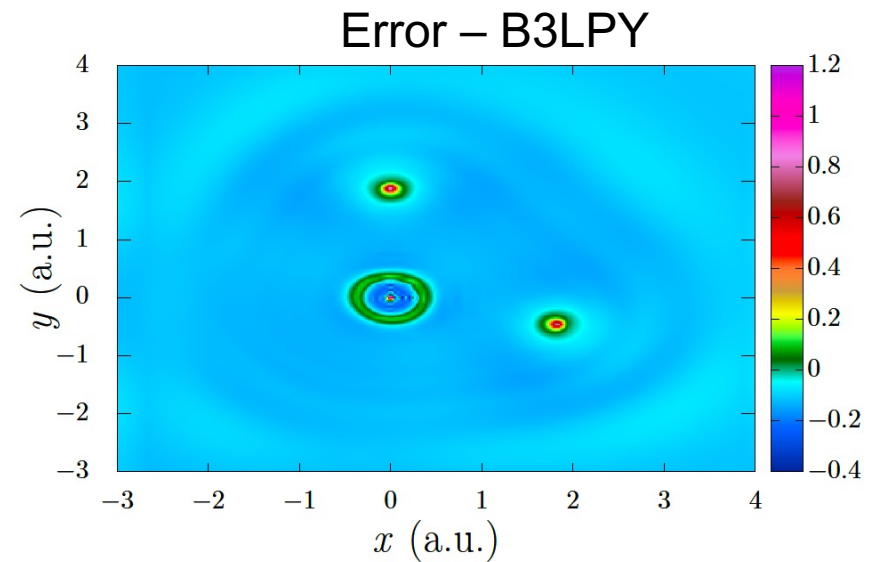
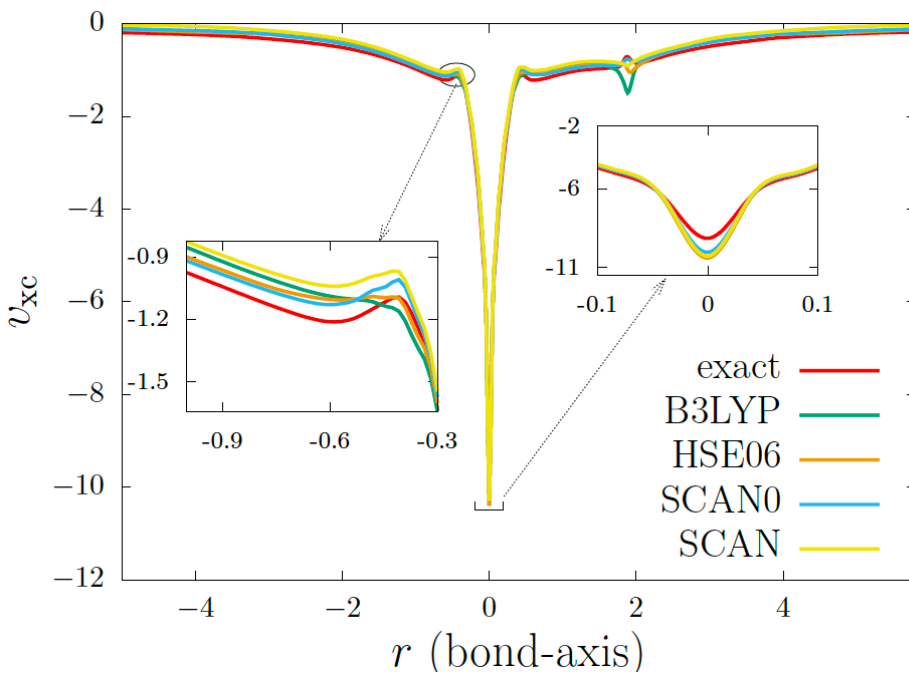


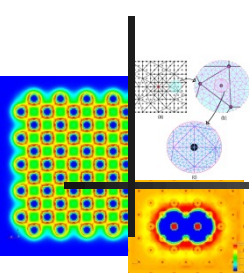
H_2 – twice equilibrium bond length





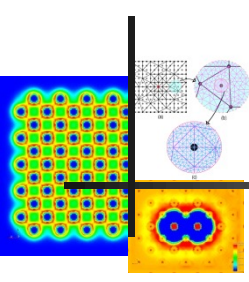
Comparison of exact XC with model XC potentials (H_2O)





Learning E_{xc}

- Express $E_{xc}[\rho] = \int e_{xc}[\rho](\mathbf{r}) d\mathbf{r}$ where $e_{xc}[\rho](\mathbf{r}) d\mathbf{r}$: energy density
- Local/semi-local models
 - $e_{xc}^{\text{LDA}}(\mathbf{r}) = e_{xc}^{\text{ML}}[\rho](\mathbf{r})$
 - $e_{xc}^{\text{GGA}}(\mathbf{r}) = e_{xc}^{\text{ML}}[\rho, \nabla\rho](\mathbf{r})$
 - $e_{xc}^{\text{near-sighted}}(\mathbf{r}) = e_{xc}^{\text{ML}}[\rho, \nabla\rho, \nabla^2\rho, g](\mathbf{r})$ $g(\mathbf{r}) = \int \rho(\mathbf{r}') k(\mathbf{r}, \mathbf{r}') d\mathbf{r}'$
- Since we do not have exact $e_{xc}[\rho](\mathbf{r})$
 - $\mathcal{L} : \sum_I \int (v_{xc}^{\text{exact}}[\rho_I](\mathbf{r}) - v_{xc}^{\text{ML}}[\rho_I](\mathbf{r}))^2 d\mathbf{r} + c \sum_I (E_{xc}^{\text{exact,I}} - E_{xc}^{\text{ML,I}})^2$
 - $v_{xc}^{\text{ML}}(\mathbf{r}) = \frac{\delta E_{xc}^{\text{ML}}[\rho]}{\delta \rho(\mathbf{r})} = \int \frac{\delta e_{xc}^{\text{ML}}(\mathbf{r}')}{\delta \rho(\mathbf{r})} d\mathbf{r}'$
 - Learning is on $e_{xc}[\rho](\mathbf{r})$, but optimization is on $v_{xc}(\mathbf{r})$



THANK YOU!

